MODIFICATION OF SOLIDIFICATION STRUCTURES BY PULSE ELECTRIC DISCHARGING

BY

MASAYUKI NAKADA

B.E. Waseda University, 1975
M.E. Waseda University, 1977

SUBMITTED IN PARTIAL FULFILLMENT OF
THE REQUIREMENT OF THE
DEGREE OF
MASTER OF SCIENCE

at the

MASSACHUSETTS INSTITUTE OF TECHNOLOGY

June, 1985

Signature of Author ______________________
Department of Materials
Science and Engineering,
May 10, 1985

Certified by ______________________
Professor Merton C. Flemings
Thesis Supervisor

Certified by ______________________
Dr. Yuh Shiohara
Research Supervisor,
Materials Processing Center

Accepted by ______________________
Professor Bernhardt J. Wuensch
Chairman, Departmental
Committee on Graduate Students

MODIFICATION OF SOLIDIFICATION STRUCTURES BY PULSE ELECTRIC DISCHARGING

BY

MASAYUKI NAKADA

Submitted to the Department of Materials Science and Engineering on May 10, 1985 in partial fulfillment of the requirement for the degree of Master of Science

ABSTRACT

A new innovative process using pulse electric discharging for modification of solidification structures was investigated in this research work.

If an extremely high voltage or high current is applied to solidifing metal alloys by discharging a capacitor bank, large pressure gradients due to the pinch force and a temperature increase caused by joule heat can be expected. When such pressure gradients and temperature increase are applied, solidification is thought to be different from usual solidification.

Serial experiments were performed for 60g of Sn-15wt%Pb alloy and the appropriate conditions to modify solidification structures were examined.

When appropriate conditions in terms of cooling rates of specimens, initial capacitor bank voltage, and time to discharge after nucleation were chosen, even one discharge could modify solidification structures from dendritic to globular. The limit to obtain globular structures could be expressed by initial capacitor bank voltage and the fraction of solid when discharging was carried out.

Computer calculation results for the effect of pulse electric discharging suggested that the required shear stresses to modify structure were in agreement with the data on the apparent yield stress in the Rheocasting process. The shear stress due to the pinch force seemed to be the major force to modify solodification structures.

Thesis Supervisor: Merton C. Flemings
Title:Department Head of Materials Science and Engineering

TABLE OF CONTENT

Content	Page
Abstract	2
Table of content	3
List of figures	4
Acknowledgement	8
Introduction	9
Literature survey	10
Preparation, set-up, and procedure of experiments	15
Results	19
Discussions	26
Conclusions	46
Proposed future work	47
Figures	48
Appendix	79
References	83

LIST OF FIGURES

1. Equilibrium phase diagram of Sn-Pb alloy. The alloy composition used in this work is indicated by an arrow.
2. The electric circuit and the arrangement of the metal and electrodes in the furnace for experiments.
3. The cooling curve of specimen. The temperatures were measured at 5mm under the top surface at the center (Cooling rate before nucleation was 10.8°C/min)
4. The solidification structures and the cooling curve which were obtained by natural solidification.
5. Secondary dendrite arm spacing vs distance from top surface. (Naturally solidified, cooling rate before nucleation was 12°C/min)
6. The solidification structures and the cooling curve which were obtained by discharges at 3200V at every 20 sec for the latter half of primary phase solidification. (twelve times dischargings)
7. The solidification structures and the cooling curve which were obtained by discharges at 3200V at every 20 sec for 15 sec to 80 sec after nucleation. (five times dischargings)
8. The solidification structures and the cooling curve which were obtained by discharges at 3200V at 10 and 30 sec after the nucleation point. (twice discharings)
9. The solidification structures and the cooling curve which were obtained by discharge at 3200V at 15 sec after nucleation.

10. The solidification structures and the cooling curve which were obtained by discharge at 3200V at 30 sec after nucleation.
11. The solidification structures and the cooling curve which were obtained by discharge at 3200V at 50 sec after nucleation.
12. Examples of globular structures of the primary phase which was modified due discharge.
13. Examples of transient structures of the primary phase which was not modified enough by discharge.
14. Examples of dendritic structures of the primary phase which was not modified at all.
15. The comparision of macroscopic structures between naturally solidified and discharged specimens.
16. The effect of intial capacitor bank voltage and time to trigger after nucleation on solidification structures (Cooling rate before nucleation was 10.3 to 11.7°C/min).

17. The effect of initial capacitor bank voltage and time to trigger after nucleation on solidification structures (Cooling rate before nucleation was 5.8 to 6.3°C/min).

18. The effect of initial capacitor bank voltage and time to trigger after nucleation on solidification structures (Cooling rate before nucleation was 17 to 19°C/min).

19. The relationship among the average grain size of the primary phase, time to trigger after nucleation and initial capacitor bank voltage (Coolig rate before nucleation =10.3 to 11.7°C/min). The sizes of dendrite arm spacing in a naturally solidified specimen are also shown for comparison.

20. Schematic illustrating of the cooling curve to define parameters for the calculation of fraction of solid during recalescence.

21. Fraction of solid vs time to trigger after nucleation.The limit to obtain globular structures due to discharge for different initial voltages are shown in the shadow area.

22. The flow chart for computer calculation for pinch force.

23. The area for numerical calculation (simulation for a half circle.

24. Measured voltage drop across the sample and the actual voltage drop due to resistance after taking into account the effect of inductance. (Discharged at 2500V at 210°C)

25. Calculated votage drop distribution (Discharged at 2500V at 210°C).

26. The calculated current density distribution. (Discharged at 2500V at 210°C)

27. Estimated temperature increase after discharging assuming heat flow is zero. (Discharged at 2500V at 210°C)

28. Two different kinds of volume elements used for calculations the of pinch force. (Top figure is for the calculation of the magnetic density at a certain point. Bottom figure is for the calculation of the interaction between magetic field and current)

29. Calculated pressure distribution due to the pinch force.

30. Apparent yield stress vs. fraction of solid. The data from the Rheocasting process are shown for comparison.

31. Transient structures which were supposed to be bent by shear stress due to pinch force.

Acknowledgements

I would like to express my thanks to my thesis advisor Professor Merton C. Flemings for his support, guidance, and encouragement to this thesis work.

I also deeply appriciate Dr. Yuh Shiohara for active discussions about my research work.

Thanks to the Solidification Group, especially, Mrs. Maria Due for her kind help when I was in trouble in my experiments, Mr. Joe Parse for his suggestion on the theoretical calculation of electromagnetics, Mr. Brian Monte Leibowitz for correcting English.

I am grateful to my wife Toshiko Nakada for her help in daily life. And I would like to dedicate this thesis to the expected baby.

Special thanks to my company, Nippon Kokan (NKK) for financial support for this study at MIT.

The financial support of NASA for my research is greatly appreciated.

Introduction

It is well known that when solidification structures of a primary phase consist of globular structures, one can expect great improvement in mechanical properties of final products such as tensile strength, toughness and so on.

Since globular crystals can move during solidification at higher fraction of solid compared with dendritic structure, mass feeding can occur to compensate shrinkage. Hence, the sound quality of cast ingot can be expected. To obtain such globular structures, various methods such as low temperature casting, seeding, electromagnetic stirring and Rheocasting, Vibration casting and so forth have been utilized in industries.

A new method which utilizes pulse electric discharge is based on a completely innovative idea different from other existing processes. The concept is simple. If pulses of extremely high a voltage or a high current is applied to liquid and/or semi solid metals, a large pressure gradient is generated in the liquid metals and the temperature increase due to joule heat can also be expected. If such temperature increase or liquid movement takes place during solidification, the solidification mechanism might be different from usual solidification.

The work presented here is the results of some experiments and calculations for understanding the fundamentals of the phenomena when pulse electric discharging is applied during solidification.

Literature survey

Several mechanisms have been well investigated to produce globular structures during solification. Those are 1) fragmentation or remelting of dendrite arms due to liquid movement; 2) coarsening phenomena based on Ostwalt ripening theory; 3) homogeneous and heterogeneous nucleation. Each topic is described in the following.

1.Fragmentation or remelting of dendrite arms due to liquid movement

It is well known that fragmentation or remelting of dendrite arms takes place when liquid moves during solidification due to forced convection or natural convection. Electromagnetic stirring has been applied to obtain globular solidification structures in many industries (1, 2). Many research works have been reported in this field.

Jackson and co-workers (3) carried out experiments of direct observation of remelting dendrite arms using cold model. They used cyclohexanol, tetrabromide or ammonium chloride solutions as an alloy system. Fluctuations caused by convection or stirring result in the existence of large numbers of nuclei in the liquid. Those are seemed to be the arms of dendrites which have melted off because of the temperature fluctuations and the convective effect. The presence of sufficient solute concentration between dendrite arms alters the melting temperature of the solid. The remelting of dendrites can occur either by recalescence of the whole system or by local recalescence produced by fluctuations due to convection. The crystals which melt off may be carried into the center of the casting by convection.

Another possibility is the mechanical effect of fluid motion (4-7). Especially turbulent motion gives rise to multiple bending of arms. Furthermore, if the force is strong enough, this can shear segments or branches mechanically. Vogel (7) mentioned the possibility of bending of arms due to eddies based on a consideration of hydrodynamics. Eddies can penetrate the boundary layer of fluid and those deform dendrite arms. Sometimes high angle grain boundaries appear due to deformation during solidification. Depending on the surface energy at liquid/grain boundary interface, the liquid penetrates to the newly formed boundary and thus releases a crystal into melt (8, 9). Vogel also mentions in another paper (10) that the solute gradient becomes steeper by stirring, because the thickness of the solute-enriched layer is reduced by stirring. In consequence, the growing solid-liquid interface is predicted to become more unstable. Therefore, observed shape stability in stir-casting must arise from higher density of growing particles.

In the case of vibration casting (11-16), a similar mechanism has been considered available for the fragmentation of solid during solidification. Grain refinement of metals has been achieved at frequencies ranging from 20c/s to ultrasonic frequencies of 20kc/s. Grain refinement is produced only when oscillations are applied during solidification process. In this case , cavitation or movement of liquid produces stress to break dendrites.

Another interesting process to refine solidification structures is the Rheocasting process (17-23). Flemings and co-workers found they could produce thixotropic slurries by mechanical agitation. They measured stress-strain relationships on partially solidified Sn-15wt%Pb alloy, using a Coutte type viscometer (17). At fraction of solid above 0.15, the metal rapidly develops resistance to shearing. The resistance, as measured by "apparent yield stress", is $2x10^6$dynes/cm^2 at 0.4 fraction of solid, and $4.5x10^6$dynes/cm^2 at 0.5 fraction of solid. The strain accommodation is by grain boundary cracking, and bending and fracture of dendrites. In samples which are sheared continuously as solidification proceeds, the shear stress required to maintain flow motion is 2 or 3 orders of magnitude lower than those required to initiate the flow. Fine grained materials deformed at lower stress and more homogeneously in liquid-solid zones and had more resistance to hot tearing defects. They also mentioned mass feeding proceeded to a later stage of solidification in fine grained alloys than in coarse grained alloys.

2.Melting off of dendrites associating with coarsening phenomena

So far three models have beenproposed to describe the coarsening phenomena during solidification. The first model (24) is that arms slightly smaller than the average disappear due to solute diffusion to large arms. The second (24) is the melting off phenomena of roots of dendrites. For example, a dendrite arm is considered whose root is slightly smaller than others and it tends to melt off from the necked region. And the third (25) is, if the tip of a dendrite arm has high curvature than others, the dendrite melt back. These three models are based on "Ostwald ripening theory" in kinetics and thermodynamically it is caused by Gibbs-Thompson effect (26), which is the equilibrium liquidus temperature is a function of curveture. If dendrite arms have high curvature (small radii), the equilibrium liquidus temperature becomes lower. In those three models, the second model is supposed to relate to grain refinement. If the arms are melted off, they can be nuclei for new crystals.

Kattamis and Flemings (27-30) found that the same ripening theory can be applied for spherical grain forming when specimens are undercooled significantly. As undercooling increased in Ni base alloy, the dendritic morphology tends to become finer until about 170K of undercooling, and at above this amount of this undercooling the dendrites structure abruptly disappears and turns out to be spherical. The size of spherical element is the order of dendrite arm spacing. They mentioned those results suggested that coarsening or ripening had a major effect on the morphology, and that spherical structures were not the results of enhanced nucleation, but the results of ripening or dendrite remelting. When the cooling rate is rapid after nucleation of undercooled melts, even high solute cores at center of the spherical can be retained.

3.Nucleation in melt

Grain refined structures will be obtained, if nucleation is significant in undercooled melt. There are two possibility to nucleate. The first is homogeneous nucleation and the other is heterogeneous (31, 32). However, from phenomenological view poit, it is not possible to undercool melt by more than several degrees, unless the melt is finely dispersed such as experiments using an emulsion technique. Even the crucible wall can assist nucleation. Materials which have some coherence of its crystal lattice with that of a nucleus, can be a good nucleation catalyst and seeding effect or epitaxial growth might be expected (33). This idea is widely used in factories (34).

Preparation, set-up, and procedure of experiments

1.Base metal

Base metal was produded by mixing of pure Sn (99.9999 %) and pure Pb. The composition of the base metal is Sn-15wt%Pb. the eutectic temperature is 183°C and the liquidus temperature is about 215°C. The phase diagram is shown in Figure 1. About 60g of base metal was used for each experiment.

2.Experimental Apparatus

Whole circuit: The whole electric circuit for the experiments is shown in Figure 2. Electric current goes through the specimen when a capacitor bank is triggered. In the same time, temperatures were measured by thermocouples and apparent voltage drops across the specimen were recorded in a digital oscilloscope.

The arrangement in an electric resistance furnace: Each base metal in a pyrex glass beaker as a crucible was placed in an electric resistance furnace. A couple of copper electrodes (3mm in diameter) were immersed all way down to the bottom of the crucible.

The details of each apparatus for the experiments are described in the followings.

Capacitor bank: A capacitor bank produced by EG&G which has F capacitance was used. It can be charged up to 5000 Volts.

Triggering gap: To charge the capacitor up to desired voltage from a commercial AC electric source, and to trigger at predetermined voltage, two kinds of triggering gaps were used. GP85-3 covers the initial capacitor bank voltage ranging from 500V to 2700V, and GP85 is for 3200V to 6000V. Each can be used up to 500 times discharge.

Thermocouples: Chromel-Alumel thermocouples (0.1mm in diameter) were used to measure temperature. The size of the tip was 1mm diameter. No bare part was remained after glass coating of the tip to avoid electrical conduction between the specimen and the thermocouples.

Digital oscilloscope: The voltage drop across the specimen was measured with a digital oscilloscope after the potential was reduced by resistors which have 220Mohm of resistance. The input impedance in the digital oscilloscope is 1Mohm . So those resistors reduce the potential to 1/220 of original values.

3.Experimental procedures

Procedure of experiments: The base metal was melted in the electric furnace and heated up to 280°C. Then the copper electrodes were immersed into the metal. To avoid chilling effect by the electrodes, they were set above the metal and preheated enough in the furnace before immersion. When the temperature went down to 270°C, Three different cooling methods were adoped to get different cooling rates.

Type 1: The power source for the electric furnace was turned off and the refractory plates on the top of the furnace were completely removed. This method gave the cooling rate about 18°C/min before nucleation.

Type 2: The power source for electric furnace was turned off and the half of the refractory plates on top of the furnace was removed. The cooling rate before nucleation was about 11°C/min by this method.

Type 3: The power source for electric furnace was reduced to 40% of the full power by slidac and the top of the furnace was closed by the refractory plates. By this method, the cooling rate before nucleation was about 6°C/min.

These three conditions were kept until solidification finished completely.

The nucleation of primary phase took place at about 208°C. After the nucleation began, discharging was carried out for different initial capacitor bank voltages. The time to trigger after nucleation varied, and if necessary, several times dischargings were also carried out.

When the temperature reached 100°C, the specimen was taken out of the furnace and sectioned along the center for metallography.

Metallography: Specimens were ground and polished with Al_2O_3 powder.

Etching reagent is mixture of 8 Ethilalcohol ; 1 Acetic acid ; 1 Nitric acid

Solidification structures were observed by a optical microscope (Leitz) along the center line in the specimens.

Results

1.Natural solidification in the furnace

1.1 Cooling curve

Figure 3 shows a typical example of the cooling curve in the case of natural solidification without any electric discharging, using cooling method of Type 2. The cooling rate before nucleation was about 10.8°C/min and nucleation temperature is 208°C, which was equivalent to an undercooling of about 7°C, since the liquidus temperature of the alloy is 215°C. Then the temperature increased due to release of heat of fusion during solidification, which is so called recalescence. The temperature increase due to recalescence was always in the range of 3 to 5°C in this experiment regardless of cooling rates. The average cooling rate after nucleation of the primary phaseto the nucleation of the secondary phase is 3.0°C/min as shown in this figure. The cooling rate before nucleation and that between two nucleation events mainly depends on cooling methos of 1, 2, 3.

1.2 Solidification structures of primary phase

Figure 4 shows the solidification structures of a naturally solidified specimen without discharging. Light regions corresponded to the primary Sn-rich phase and the dark regions surrounding the primary phase were eutectic phases. The primary phase appeared to be typical dendritic structures which were usally observed in conventional commercial ingots. Average secondary dendrite arm spacings were measured and shown in Figure 5. Almost all position observed except near the bottom shows around 70μm of arm spacing. In general, the secondary dendrite arm spacings are expressed in the form of equation (1) based on "Ostwald ripening theory".

$$d = A\,t^{\frac{1}{3}} \qquad (1)$$

d : secondary dendrite arm spacing

A : constant

t : local solidification time

Log of secondary dendrite arm spacing is propotional to log of local solidification time t . From this theory local solidification time of primary phase was almost same in everywhere except near the bottom. And according to another temperature measurements in naturally solidified specimen, solidification of primary phase started within a few seconds delay at 5mm and 10mm from the top surface. These facts may imply taken as an evidence that the temperature measurement at 5mm under the surface represents all over the location along the center line except near the bottom. Since the cooling condition near the bottom can not be controlled well in the electric furnace, the fraction of solid there can not be controlled either. As described later, the fraction of solid, when discharging is carried out, is a very important factor to modify solidification structures. Therefore, the microstructure will be focused in the region of 0 to 15mm from the surface.

2.Results of discharging experiments

1) Experiments to determine discharging timing

Serial experiments which roughly determine the appropriate discharging timing during solidification are described in this section.

Dischargings were applied in the latter half of solidification period of the primary phase. The cooling type (2) was used in this series to determine whether or not that discharging method was relevant. The cooling curve with discharged timing and solidification structures are shown in Figure 6. Although 12 times discharging at 3200V were carried out at every 20 second, no significant modification in microstructures was observed. The typical dendritic structures were observed which are similiar to the naturally solidified specimen as shown in Figure 4 .

Figure 7 shows the solidification structures and the cooling curve when five times discharges at every 20 sec were carried out immediately after nucleation of the primary phase at 3200V. Although the discharging in the later period had no effect to modify the solidification structures as described above (see Figure 6), the effect of discharge immediately after nucleation is significant and no dendritic structures can be observed except near the bottom. The modified structures of primary phase consisted of globular morphologies similar to those in Rheocast

Figure 8 , and Figure 9 show the solidification structures in the specimens which were discharged twice or once after nucleation at 3200V of intial capacitor bank voltage respectively. The structures observed are still globular as well as 5 times discharged specimen in Figure 7 .

Figure 10 and Figure 11 show the solidification structures when only one discharging was carried out at 30sec and 50sec after nucleation at 3200V,respectively. These structures indicate those discharging timing were too late to modify the solidification structures, since the typical dendritic structures exist all over the specimens.

It could be concluded that discharging immediately after nucleation is necessary to modify the structures, and even only one discharging can modify the solidification structures from dendritic to globular significantly.

2)The effect of initial capacitor bank voltage and cooling rate before discharging.

A serial of experiments were carried out to understand the effect of initial capacitor bank voltge and cooling rate before discharge.

Before the description of those results, some standards of solidification structures are shown in Figure 12,13,and 14 with which the modification of solidification structures was evaluated. When appropriate discharging voltage and discharge timing during solidification of the primary phase were chosen, the structures become globular as shown in Figure 12 . However, if the conditions to modify were off the appropriate conditions, transient structures were observed. Those structures have different appearences from somewhat globular or somewhat dendritic structures as shown in Figure 13. And finally when the discharging conditions were not appropriate, typical dendritic structutres can be observed as shown in Figure 14. The comparison of macroscopic structures are shown in Figure 15. Apparently very coarse grains could see in the naturally solidified specimen. On the other hand, grains observed macroscopically were extremely fine in the specimen which was discharged at 3200V at 15 sec after nucleation.

The results which are appreciated solidification structures based on those standards are shown in Figures 16, 17, and 18. Each pltot is the average of the points at 5mm and 10mm under the top surface. Each figure was obtained under different cooling rate experiments. Figure 16 is the results of the experiments which have cooling rates of 10.3°C to 11.7°C/min before nucleation (type 2 cooling). The tendency of these results is that the solidification structures tend to be globular as initial capacitor bank voltage increases and the structures becomes dendritic as time to discharge (trigger) after nusleation increases. The area which is depicted as circular plots in Figure 16 is appropriate to modify structures. Figure 17 is the results of the experiments which have cooling rates 5.8°C to 6.3°C/min before nucleation (type 3 cooling). Although these results show the same tendency as Figure 16 , the appropriate area to modify structures shifts down a little from Figure 16. In other words, the structures can be modified at lowerer intial capacitor bank voltage when lower cooling rates applied. Figure 18 shows the results of experiments whose cooling rate was 17 to 19°C/min before nucleation (type 1 cooling). The tendency itself in the figure is similar to Figure 16 and Figure 17. However, it becomes extremely difficult to modify structures at low initial capacitor bank voltage.

Figure 16, 17 and 18 explained above are relatively qualitative expressions in terms of solidification structures, because those evaluation of structures were based on the arbitrarily chosen standards which mentioned already. To avoid such ambiguity, the average size of primary phase was measured at the same points from the specimen whose cooling rate before nucleation was 10.3°C to 11.7°C/min (type 2 coolig), as shown in Figure 19. The different kinds of plots show the individual initial capacitor bank voltage and solid (black), open and half open (half black) indicated globular, dendritic or transient structures respectively. The average grain size of primary phase becomes larger as the time to trigger after nucleation increases with even the same capacitor bank voltage, and the structures tend to change from globular to transient or from transient to dendritic as well. When discharge was carried out at a higher initial capacitor bank voltage, the average grain size of the primary phase became smaller and structures changed from dendritic to transient or from transient to globular. Another interesting point is comparison between modified structures and secondary dendrite arms of naturally solidified specimen. The cooling rate before nucleation in the naturally solidified specimen was 12o^{C}/min. The rate was an almost same value as discharged specimens. When solidification structures were modified well such as the structures which were obtained by the discharge at 3200V, those sizes reachedto the size of secondary dendrite arm lengths or thicknesses.

Discussions

In previous sections, the relationship between solidification structures and three factors was described, which are initial capacitor bank voltage, cooling rates and time to trigger (discharge) after nucleation. The important point is to find what exists behind those three factors. To answer this question, fraction of solid at discharging was estimated and the relationship between fraction of solid and modification of structures will be examined. Secondly, temperature increase due to joule heating calculated by a numerical method will be explained. Thirdly, the estimated shear stress by a pinch force calculation will be compared with the data of the Rheocast process, whose effect on modification of solidification structures is thought to be due to shear stress mainly.

1. Estimation of fraction of solid at discharge and the relationship between fraction of solid and modification of solidification structures.

At first, the typical example of cooling curve is shown in Figure 20. T_i and t_i are the temperature and the time at an initial point. T_n and t_n are at nucleation, T_d and t_d are at discharging, respectively. Dischargings were always carried out during recalescence period. The heat extraction before nucleation began is expressed by equation (2) assuming Newtonian cooling. This assumption is valid at slow cooling rates. The specimens were cooled in the electric furnace, and the surrounding of the specimen is pyrex glass except the top surface. Therefore, the cooling condition is supposed to be very close to the Newtonian cooling. And assuming that heat flux was kept constant after nucleation, the heat balance after nucleation to discharging point can be expressed by equation (3). Equation (3) indicate the heat release due to solidification (heat of fusion) is equal to the sum of temperature increase (heat capacity) and heat extraction. Combining equation (2) and (3) gives equation (4). And assuming density of liquid and solid are the same (turns out to be volume of liquid and solid are very close to each other), specific heat of liquid and the average specific heat of solid and liquid are very close to each other, the equation (5) can be derived. All values are known except f_s (weight fraction of solid when discharged). Therefore, f_s can be readily calculated. Figure 21 shows the relationship between calculated fraction of solid and time to trigger (discharge) after nucleation. When experiments were carried out, solidification structures, initial capacitor bank voltage, time to trigger after nucleation and cooling curve were known. The upper limits to modify the solidification structures to globular at certain initial capacitor bank voltages could be estimated. The cooling rate before nucleation in Figure 21 was the average value of each point, whose cooling rate are very close each other. The interesting point is that the upper limits to modify the solidification structures to globular give the almost the same fraction of solid, even if the cooling rates differs, and that the upper limits became larger fraction of solid when initial capacitor bank voltage was raised.

1)ESTIMATION OF HEAT EXTRACTION(ASSUMING NEWTONIAN COOLING)

$$QA=\frac{1}{t_N-t_i}\cdot\int_{T_N}^{T_i}\rho_L V\ C_L dT \tag{2}$$

2)HEAT BALANCE DURING RECALESCENCE

$$\int_0^{f_s^d}\rho_s V\ \Delta H df_s= QA(t_d-t_N)+\int_{T_N}^{T_d}\bar{\rho}\ V\bar{C}dT \tag{3}$$

$$\int_0^{f_s^d}\rho_s V\ \Delta H df_s=\left(\frac{t_d-t_N}{t_N-t_i}\right)\int_{T_N}^{T_i}\rho_L V\ C_L dT+\int_{T_N}^{T_d}\bar{\rho}\ V\bar{C}dT \tag{4}$$

WHEN $\rho_S \simeq \rho_L$, $C_L \simeq \bar{C}$

$$\Delta H f_s^d = \left(\frac{t_d-t_N}{t_N-t_i}\right)C_L(T_i-T_N)+C_L(T_d-T_N) \tag{5}$$

WHERE C_L= 0.073cal/g deg,ΔH= 17 cal/g

Q:Heat flux to outside from the boundary

A:Area of boundary

T_i,t_i:Temperature and time of initial point

T_d,t_d:Temperature and time at discharge

T_N,t_N:Temperature and time at nucleation

ρ_L,V ,C_L:Density,volume and specific heat of liquid

ρ_S, f_s :Density, and fration of solid

$\bar{\rho}$, $\bar{C}$:Density, and specific heat of average of liquid and solid

ΔH:Heat of fusion

2. Numerical calculation of potential distribution, current density distribution, temperature increase due to joule heat and estimation of decrease of fraction of solid caused by temperature increase.

2.1 Potential distribution and current density distribution (35, 36, 37)

2.1.1 Basic equations

At first, basic equations to calculate potential distribution and current density distribution across the liquid specimen are described. Conservation of potential is written as equation (6). This is so called the "Laplace equation". Originally, the right hand side term is not zero if it is non-steady state. Nonetheless, in metals charging disappers very quickly because the diffusion rate of electrons are extremely rapid. So the Laplace equation is applicable to this calculation. Once potential distribution is known , the current density can be calculated by equation (7). That is so called the "Ohm's law". Consevation of current must be satisfied simultaneously as shown by equation (8). However, if equation (6) and equation (7) are taken into account in togother, equation (8) must be readily satisfied.

CALCULATION OF POTENTIAL AND CURRENT DISTRIBUTION

1. FUNDAMENTAL EQUATIONS(STEADY STATE)

1)CONSEVATION OF POTENTIAL

$$\frac{\partial^2 E}{\partial X^2} + \frac{\partial^2 E}{\partial Y^2} = 0 \qquad (6)$$

2)OHM'S LAW

$$\frac{\partial E}{\partial X} + \frac{\partial E}{\partial Y} = -\frac{I}{\sigma} \qquad (7)$$

3)CONSERVATION OF CURRENT

$$\frac{\partial I_x}{\partial X} + \frac{\partial I_y}{\partial Y} = 0 \qquad (8)$$

2. BOUNDARY CONDITIONS

1)VERTICAL DIRECTION TO BOUNDARY

$$(\sigma_m \vec{E}_m - \sigma_g \vec{E}_g) \cdot \vec{N} = 0 \qquad (9)$$

2)PARALLEL DIRECTION TO BOUNDARY

$$(\vec{E}_m - \vec{E}_g) \cdot \vec{t} = 0 \qquad (10)$$

3)VOLTAGE DIFFERENCE ACROSS THE SPECIMEN
AFTER TAKING ACCOUNT OF INDUCTANCE

$$V_E = V_S + L\frac{dI}{dt} = IR_S + L\frac{dI}{dt} \qquad (11)$$

$E = V_S$ IN EQATION (6)

Where

E:Potential

I:Current

σ:Electric coductivity

I_x:Current in X direction

I_y:Current in y direction

σ_m, σ_g:Electric coductivity of metal and glass

$\vec{E}_m, \vec{E}_g$:Potential vector in metal and glass near the boundary

$\vec{N}$:Unit vector in vertical direction to the boundary

$\vec{t}$:Unit vector in parallel direction to the boundary

V_E:Measured voltage drop between electrodes with a digital oscilloscope

V_s:Voltage drop due to resistance in the specimen

L:Inductance coeffecient (measured value: 0.040 mH)

t:Time

2.1.2 Boundary conditions

Boundary conditions are written in equation (9) and (10). Equation (9) predicts that the potential drop in the metal near the boundary (between metal and glass)is negligible, since the electric conductivity of the glass can be assumed to be zero at the temperatures of interest (about 200°C). And equation (10) implies that potential drop along the boundary between metal and glass must be the same. That is satisfied when the boundary has the same potentials to metal and glass. Another required boundary condition is to determine the actual votage drop across the specimen. As shown in Figure 2 in previous section, the apparent voltage drop across the specimen was measured by a digital oscilloscope without difficulties. However, these measured values include, not only actual voltage drop due to resistance, but due to inductance, because AC is always observed as a characteristic of capacitors. Using equation (11) the actual voltage drop due to resistance was calculated and the actual voltage drop should be substitued to equation (6) to evaluate the potential distribution.

2.1.3 FINITE DIFFERENTIAL EQUATIONS FOR THE CALCULATION OF POTENTIAL DISTRIBUTION AND CURRENT DISTRIBUTION

1)POTENTIAL(FROM EQUATION 5)

$$\frac{E(X+DX,Y) + E(X-DX,Y) - 2E(X,Y)}{DX^2} + \frac{E(X,Y+DY) + E(X,Y-DY) - 2E(X,Y)}{DY^2}$$

$$= \quad 0 \qquad \text{-----------} \ (12)$$

$$E(X,Y) = \frac{DY^2(\ E(X+DX,Y)+E(X-DX,Y)\ ) + DY^2(\ E(X,Y+DY) + E(X,Y-DY)\ )}{2\ (\ DX^2 + DY^2\ )}$$

$$\text{------------} \ (13)$$

2)OHM'S LAW (FROM EQUATION 6)

$$\frac{E(X+DX,Y) - E(X-DX,Y)}{2DX} + \frac{E(X,Y+DY) - E(X,Y-DY)}{2DY} = -\frac{I(X,Y)}{\sigma}$$

$$\text{-------------}(14)$$

$$I(X,Y) = \sigma\cdot\left[-\frac{1}{DX}E(X+DX,Y) + DX\left(\frac{1}{DX^2} + \frac{1}{DY^2}\right)E(X,Y) \right.$$
$$\left. -\frac{DX}{2}\left(\frac{1}{DXDY} + \frac{1}{DY^2}\right)E(X,Y+DY) + \frac{DX}{2}\left(\frac{1}{DXDY} - \frac{1}{DY^2}\right)E(X,Y-DY)\right]$$

$$\text{--------------}(15)$$

DX,DY = length of each segement in x,y direction

$$Vs = V_E - L\frac{dI}{dt} = V_E - L\frac{I-I'}{\Delta t} = I \cdot R \qquad (16)$$

I:the new current after Δt

I':the current before Δt

Where Vs was determined before calculation of potential distribution and current density, and was utilized as boundary condition at the electrodes (one electrode is at Vs and the other is zero).

2.1.4.Flow chart for numerical calculation

The flow chart for numerical calculation for the potential distribution and current density distribution is shown in Figure 22.

At first the data were stored such as R (resistance of each segment), DX, DY (distance between each segment), and ERR (reference error). Secondary, initial conditions were fixed in terms of initial potential values to avoid making an error to substitue zero into denominators in the calculation. And boundary conditions were fixed. According to those input values new potential values were calculated. If the errors between new potential values and old potential values were smaller than ERR which was given as 0.0001, calculation went to convergence and if not, it returned to fix the boundary conditions and continued to calculate new potential values until enough convergence was obtained. When it converged, current density distribution was calculated based on the calculated potential distribution. Using a current density value in each segment, pinch force was calculated. The details of the calculation for the pinch force are described later in this section.

2.1.5.Calculation area

The calculation area is shown in Figure 23 , which is surrounded by thick lines. It covers a half of the specimen , because of a symmetric configuration of the specimen and the boundary is expressed by steps, although the actual boundary is smooth and a part of a circle. As integration of current density in x direction was required for further calculation, cylindrical coordinate could not be applied in this calculation. The area consists of 20 points in x direction and 39points in y direction in segments. And the two electrodes exist at (1, 1) and (1, 39).

2.1.6.Measured voltage drop across the specimen and the actual voltage drop due to resistance.

Figure 24 shows the measured voltage drop across the sample by a digital oscilloscope when discharged at 210°C at initial capacitor bank voltage of 2500V. The figure shows the a typical resonance and the discharge lasts for about 1 millisecond. The maximum voltage drop was 165V. However, the actual voltage drop due to resistance was very small and the order of magnitude was 10^{-3}volts. The actual voltage drop due to resistance was calculated by equation (16) using measured voltage by digital oscilloscope. And a little phase shift could be realized, if compared both figures. The maximum voltage drop due to resistance was 7.7×10^{-3}V .

2.1.7 Calculated potential distribution and current density distribution

Figure 25 shows the potential distribution when 7.7×10^{-3}V was used as voltage drop across the spcimen due to resistance. That value was the maximum when discharged at 2500V.

Figure 26 shows the current density distribution which was calculated using the potential distribution as shown in Figure 25. The order of the current density was hundreds to thousands ampere/cm^2.

2.2.Temperature increase due to joule heat

From Figure 24-2), the average voltage during discharging was estimated. Then the average current density was also calculated, since the resistance of specimen was estimated as listed in Apendix (1). That turned out to be joule heat accumulation during discharging. The configuration of distribution of joule heat accumulation was exactly same as the current distribution . The joult heat accumulation was calculated by eqution (17):

$$W=I^2Rt \tag{17}$$

where

W:joule heat accumulation during discharge

I:average current density in a unit segment

R:resistance in a unit segment

t:diacharging time

The temperature increase due to joule heat during discharging is shown in Figure 27 , assuming no existence of solid. The order of the temperature increase is of 10^{-2} to 10^{-4}°C.

$$T= \frac{W}{4.2\ C_L\rho} \tag{18}$$

where

C_L:specific heat of liquid

ρ:specific density

The temperature increase was very small except near the electrodes. However, it remained uncertainly that the joule heat to give the temperture increase of 10^{-2} to 10^{-4}°C could remelt the root of dendrites and those turned out to be a seperated solid. If the heat balance to evaluate the decrease of fraction of solid due to joule heating was considered, the following equation was derived.

$$-\int_{f_s^b}^{f_s^a} \Delta H df_s + \int_{T^b}^{T^a} \bar{C}_p dT \qquad = W \qquad (19)$$

$$= -\Delta H(fs^a - fs^b) + C_p(T^a - T^b) \qquad (20)$$

$\Delta H = 1.7 Kcal/mol \approx 17 cal/g$

$C_p = 7.3 cal/mol \approx 0.073 cal/g\, deg$

$$W = 17(fs^b - fs^a) + 0.073(T^a - T^b) \qquad (21)$$

where

H;heat of fusion

Cp:specific heat

fs^a:fraction of solid after discharge

fs^b:fraction of solid before discharge

T^a:temperture after discharge

T^b:temperture before discharge

Assuming the second term in equation (21) equals to zero to get the hypothetical maximum value of the $17(fs^b - fs^a)$ term. From the numerical calculation , the highest joule heat accumulation during discharging is the order of 0.0442joule/cm^2 near by the electrodes, which resulted in $fs^b - fs^a = 0.0006$. When the fraction of solid before dischrging is 0.02 (from Figure 21), the difference between after and before the discharge was extremely small and solid was very hard to be remelted by the joule heating.

Another important effect of curvature of dendrite arms was completely ignored in this calculation. There was still a possibility remained to remelt the root of dendrite arms due to curvature effect associated with the small temperature increase.

2.3. Calculation of pressure distribution due to pinch force and estimation of shear stress (35-37)

2.3.1. Calculation of pressure distribution due to pinch force

So called pinch force is generated by the interaction between current and magnetic field at a point. Therefore, it is necessary to estimate current and magnetic fields at a point. Consider one volume element in the specimen as shown in Figure 28 , whose vertical surfaces are along the potential line (current flows in this line). Since the current I in the volume element was already known by the calculated current density distribution, the magnetic density on the vertical surface was calculated by equations (22) and (23), assuming a cross section of the volume element, which was vertical to current flow, was a part of a long plate. And if another small volume element on the vertical surface of the larger volume element was considered, the current through which was expressed by equation (24). The pinch force

CALCULATION OF PINCH FORCE

1. MAGNETIC DENSITY AT IMAGINARY SURFACE ALONG POTENTIAL LINE

$$H = 2\pi I \tag{22}$$

$$B = \mu_0 H = 2\pi\mu_0 I \tag{23}$$

WHERE $I = 2\int_0^x i(X)\cdot dx$

2. CURRENT IN VOLUME ELEMENT AT THE IMAGINARY SURFACE

$$di = i(X)\cdot dX \tag{24}$$

3. PINCH FORCE ON VOLUME ELEMENT AT THE IMAGINARY SURFACE

$$df_x = B di\cdot dl\cdot \cos(\frac{\pi}{2}-\Theta) \tag{25}$$

$$df_y = B\, di\cdot dl\cdot \cos(\frac{\pi}{2}-\Theta) \tag{26}$$

$$dP_x = -\frac{df_x}{d\ell\cdot 1} = -B\cdot di\cdot \cos(\frac{\pi}{2}-\Theta) \tag{27}$$

$$dP_y = -\frac{df_y}{d\ell\cdot 1} = -B\cdot di\cdot \sin(\frac{\pi}{2}-\Theta) \tag{28}$$

Where

I:current

H:magnetic flux

B:magnetic density

X:distance in x direction

di:current through a small volume element with thichness of dx

i(x):current density at x

dl:length of a small volume element

df_x:pinch force at a small volume element in x direction

df_y:pinch force at a small volume element in y direction

Θ:angle of a small volume element to the cross section of a large volume element

dP_x:pressure due to pinch force in x direction at a small volume element

dP_y:pressure due to pinch force in y direction at a small volume element

μ_o:magnetic permeability in liquid metal was calculated by the interaction between the current expressed by equation (24) and the magnetic density expressed by equation (23). The pinch forces are expressed by equations (25) and (26) for x and y directions respectively. If these equations were devided by $dl'xl$, the pinch force turned out to be pressure as shown by equations (27), and (28). When θ was obtained by the assumption which is that potential lines consist of parts of circles which went in between electrodes (See appendix 2). The calculated results are shown in Figure 29, which were obtained by using the actual voltage drop across the specimen , i.e., $7.7x10^{-3}$V. That was the maximum voltage drop due to resistance, when discharged at 2500V. It is of interest that the arrows of pressure vectors are facing towards the center of the specimen. The motion of the surface of the specimen near the center (rise of the surface at the center) was always observed when discharged. Both the observation and the calculation results have a good agreement qualitatively.

2.3.2.Estimation of shear stress due to pressure difference

The force distribution which exerted on each small volume elements was calculated from the calculated pressure distribution. The velocity differnce was roughly estimated by equation (29), using the force distribution .

$$\Delta Ft=m\Delta v \qquad (29)$$

ΔF:force difference

t:time(=0.1msec)

m:mass of segment (=8.75×10^{-3}g)

Δv:velocity differnce in fluid

Assuming a Newtonian fluid , shear stress due to velocity gradient of fluid is expressed by

$$\tau_x=-\eta\frac{\partial v_x}{\partial y} = -\eta\frac{\Delta v_x}{\Delta y} = -\eta\frac{\Delta F_x t}{\Delta y m} \qquad (30)$$

$$\tau_y=-\eta\frac{\partial v_y}{\partial x} = -\eta\frac{\Delta v_y}{\Delta x} = -\eta\frac{\Delta F_y t}{\Delta x m} \qquad (31)$$

η:viscosity (=0.05poise)

$\Delta x,\Delta y$=0.05cm

$\Delta F_y,\Delta F_x$=2000~6000 dyne/cm^2 when discharged at 2500V

Therefore, the average of τ x, τy is 4400dyne/cm^2 when discharged at 2500V. The fraction of solid, voltage drop due to resistance (which gave a rough estimation of shear stress), and the solidification structutures were investigated. The estimation of the shear stress , when structures observed were at the border between globular and transient, was compared with the apparent yield stress which Flemings and co-workers mentioned in their paper (17). Based on that idea, the data which were obtained empirically are plotted in Figure 30 , and some data which obtained by Rheocasting process are also shown for comparison (the alloy composition for the Rheocast experiment was the same as this experiment, i.e. Sn-15wt%Pb).

Although the shear stresses were roughly estimated in this experiment and calculations, those data were on the extention of the data of Rheocasting and showed relatively good agreement with Rheocasting process. It might be concluded the mechanism to modify solidification structures was very close to Rheocasting process. So it was thought the mechanism to modify solidification structures were mainly attributed to the shear stress due to the pinch force. Figure 31 shows an example of transient structures. A dendrite structure at the center of the picture seemed to be bent due to the shear stress.

Conclusions

1. Solidification structures can be modified by pulse electric discharging with a capacitor bank. If appropriate conditions are chosen, even a single discharge can modify the solidification structures significantly.

2. The appropriate conditions to modify solidification structures are described in terms of initial capacitor bank voltages, time to trigger after nucleation, and cooling rates.

3. The effect of the time to trigger after nucleation and the cooling rate can be converted to the fraction of solid. The upper limits of fraction of solid to modify the structures at a specific initial capacitor bank voltge have almost the same values, even when the cooling rate and time to trigger are different. Higher initial capacitor bank voltages are required to modify structures when discharing is carried out with a higher fraction of solid.

4. The roughly estimated shear stress to modify solidification structures have a relatively good agreement with the data on the apparent yield stress in the Rheocasting process reportedly. The mechanism of modification of structures is supposed to be mainly the shear stress due to the pinch force. However, the possibility of remelting the roots of dendrite arms has remained as unknown factor.

Proposed future work

1. Shorter time to trigger after nucleation, for example 0 sec to 10 sec at various initial capacitor bank voltges should be carried out. This work might be helpful to find the limit of melting dendrites due to joule heating.

2. The effect of mass of specimens should be investigated.

3. The effect of the configuration of specimens and electrode should be considered.

4. More detail about the mechanism to modify structures should be investigated.

5. Experments with higher temperature alloys such as steels and cast irons should be carried out.

6. Application for industrial processes should be considered.

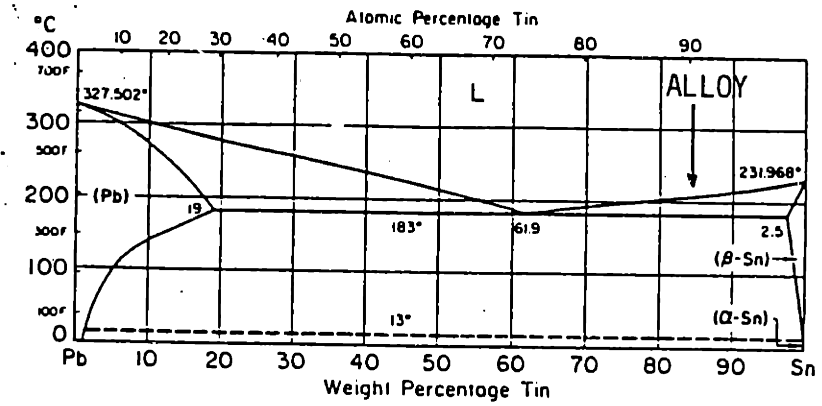

Figure 1. Equilibrium phase diagram of Sn-Pb alloy.

The alloy composition used in this work is indicated by an arrow.

1)Circuit

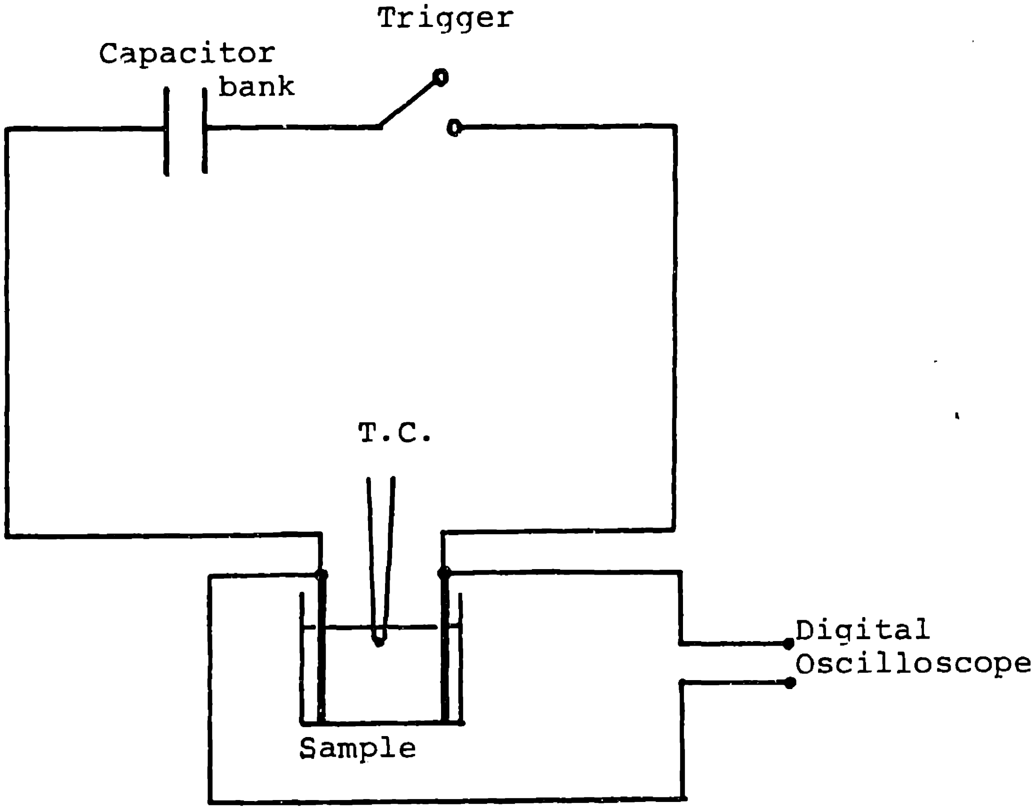

2)Arrangement in the furnace

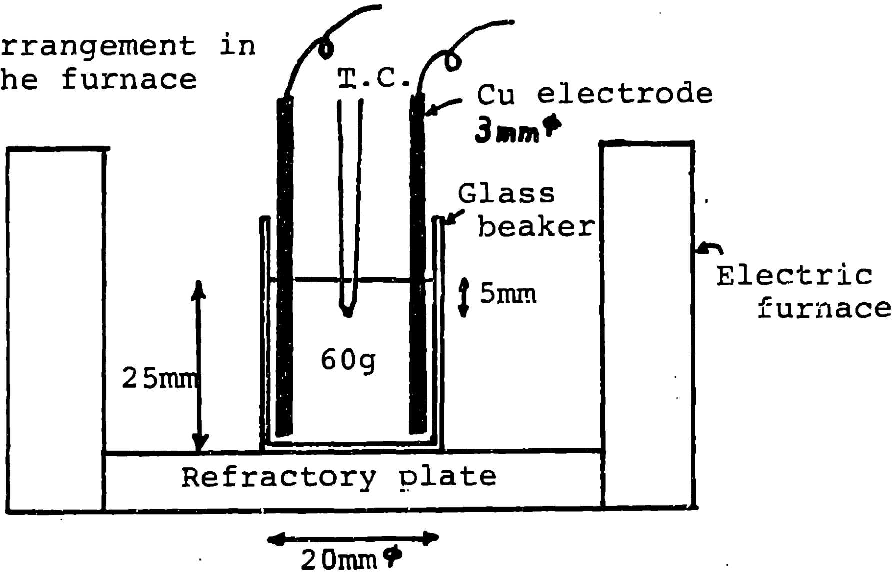

Figure 2
The electric circuit and the arrangement of the metal and electrodes in the furnace for experiments .

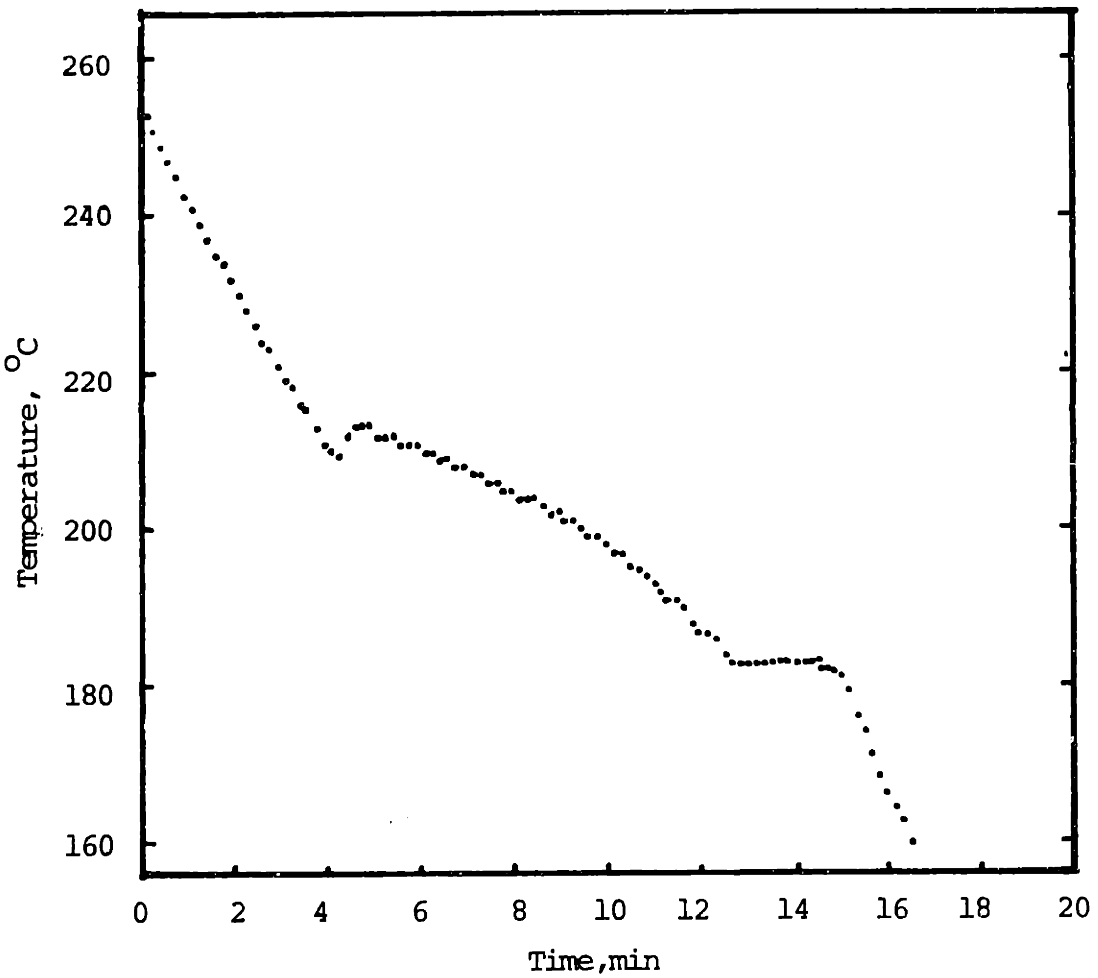

Figure 3 The cooling curve of spcimen. The temperature was measured at 5mm under top surface at the center (Cooling rate before nucleation =10.8^{O}C/min)

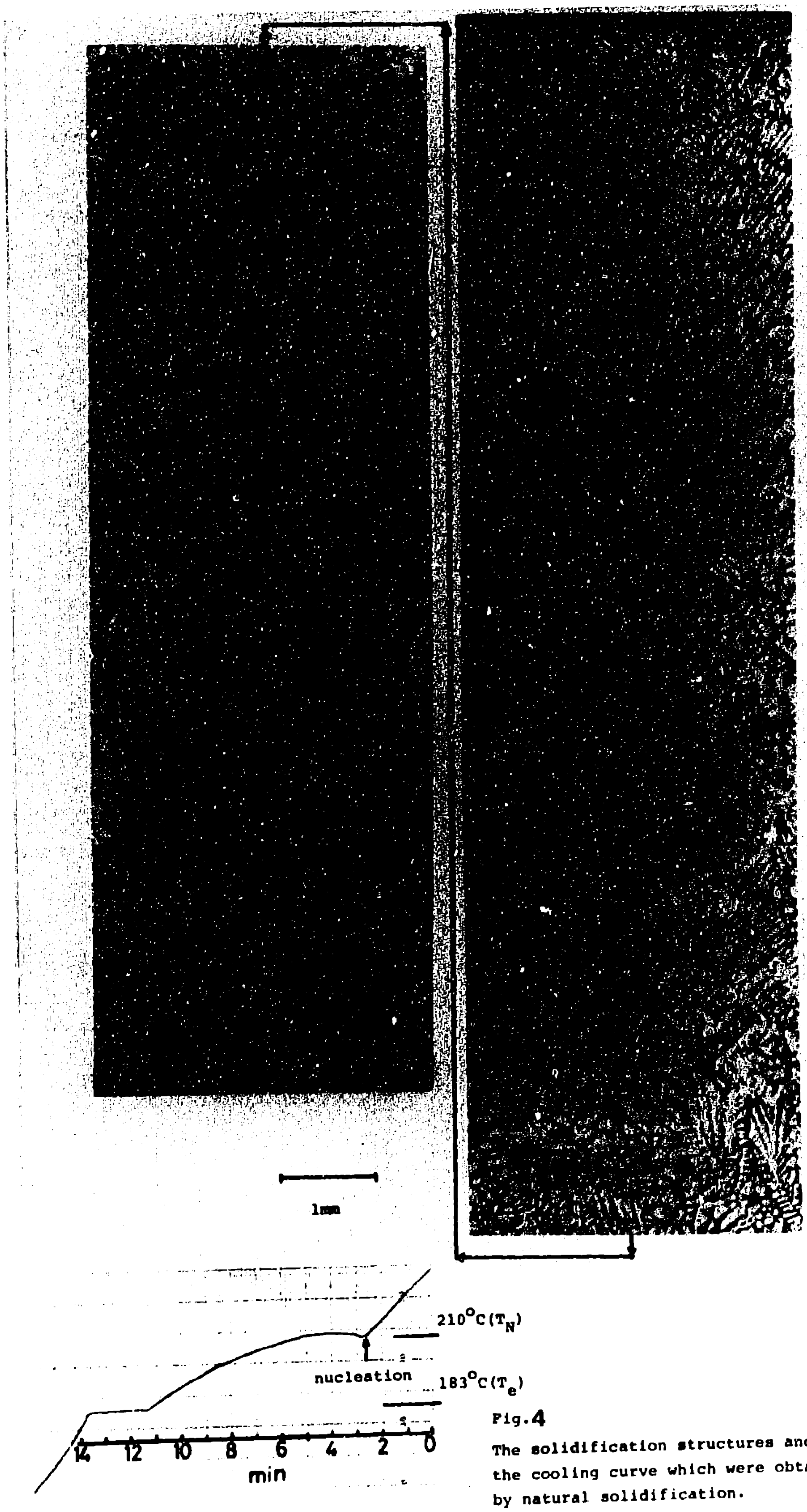

Fig.4

The solidification structures and the cooling curve which were obtained by natural solidification.

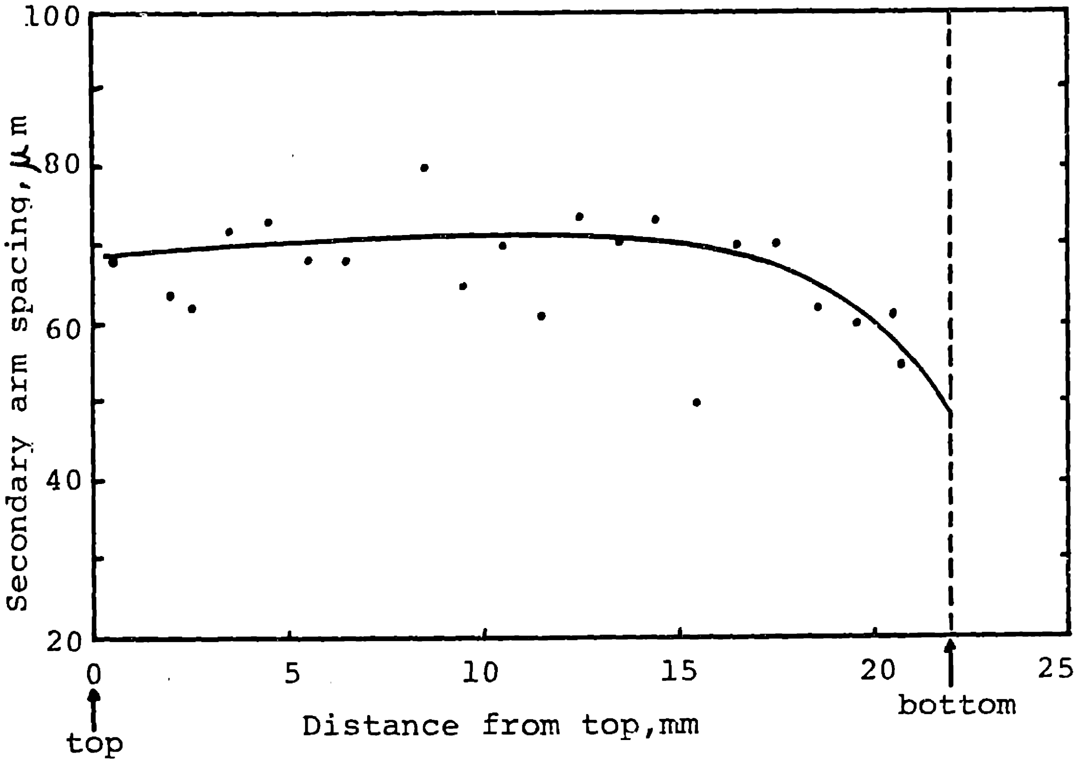

Figure 5 The secondary dendrite arm spacing vs. the distance from the top surface. (naturally solidified,cooling rate before nucleation was 12°C/min)

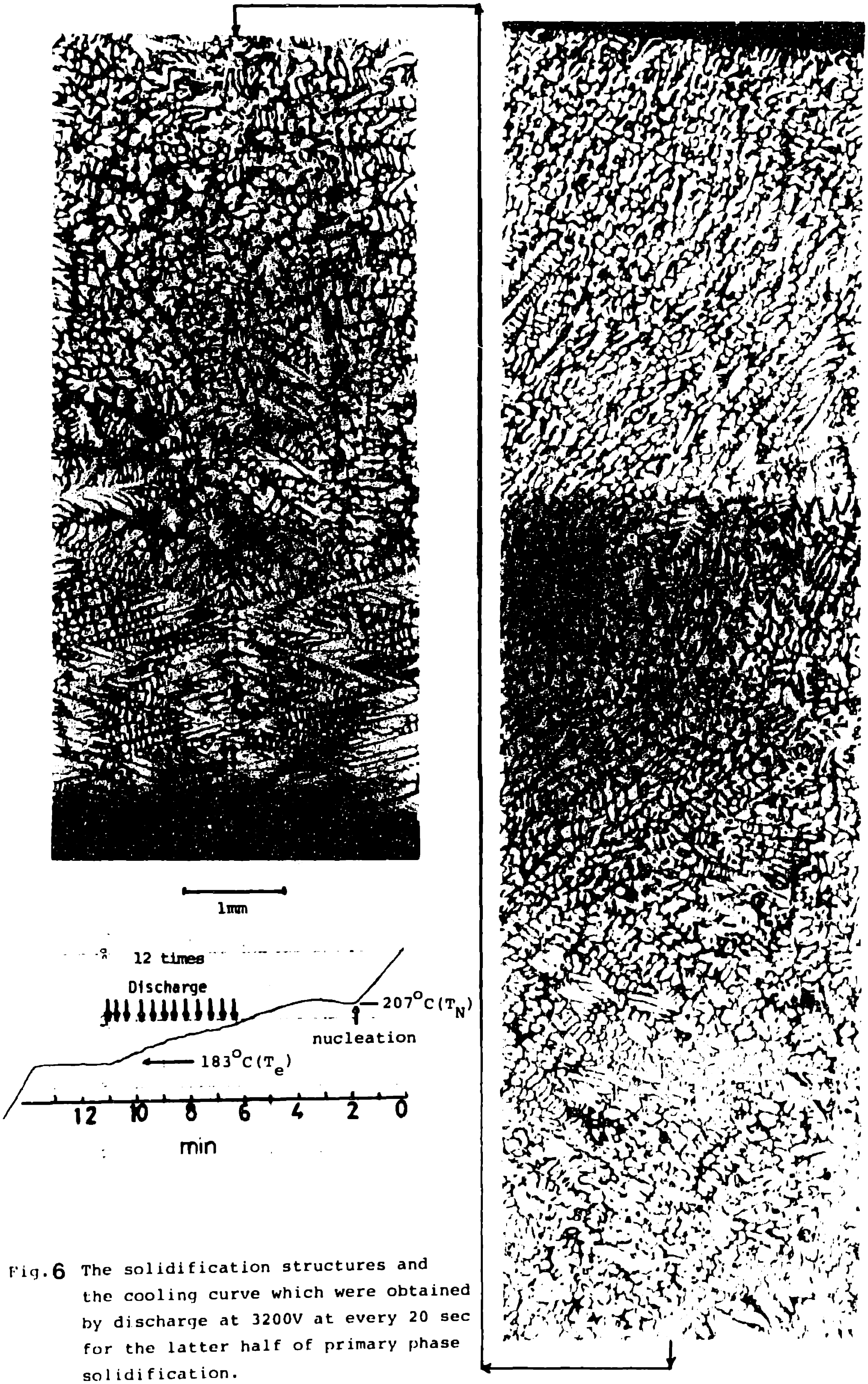

Fig.6 The solidification structures and the cooling curve which were obtained by discharge at 3200V at every 20 sec for the latter half of primary phase solidification.

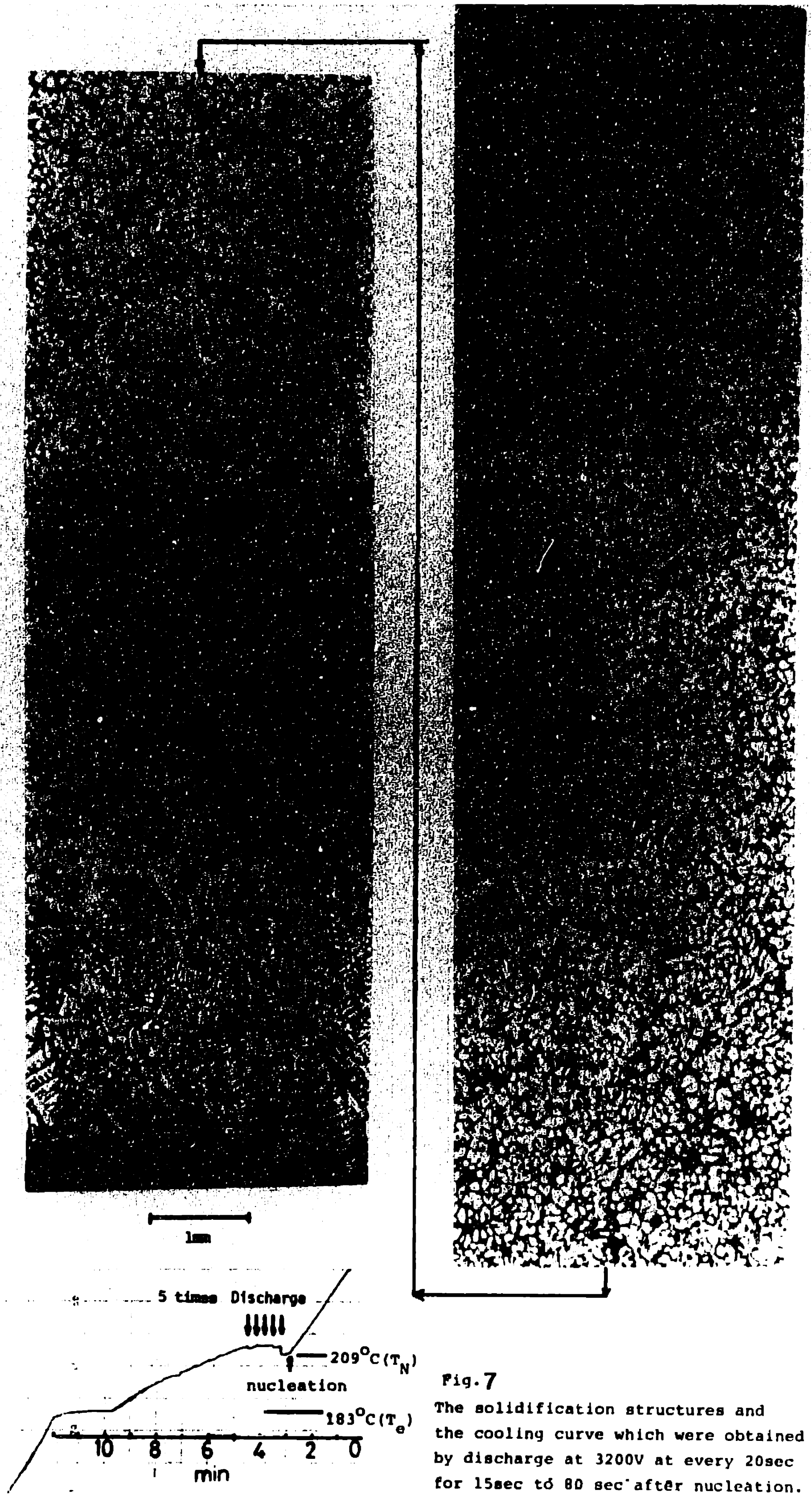

Fig. 7

The solidification structures and the cooling curve which were obtained by discharge at 3200V at every 20sec for 15sec to 80 sec after nucleation.

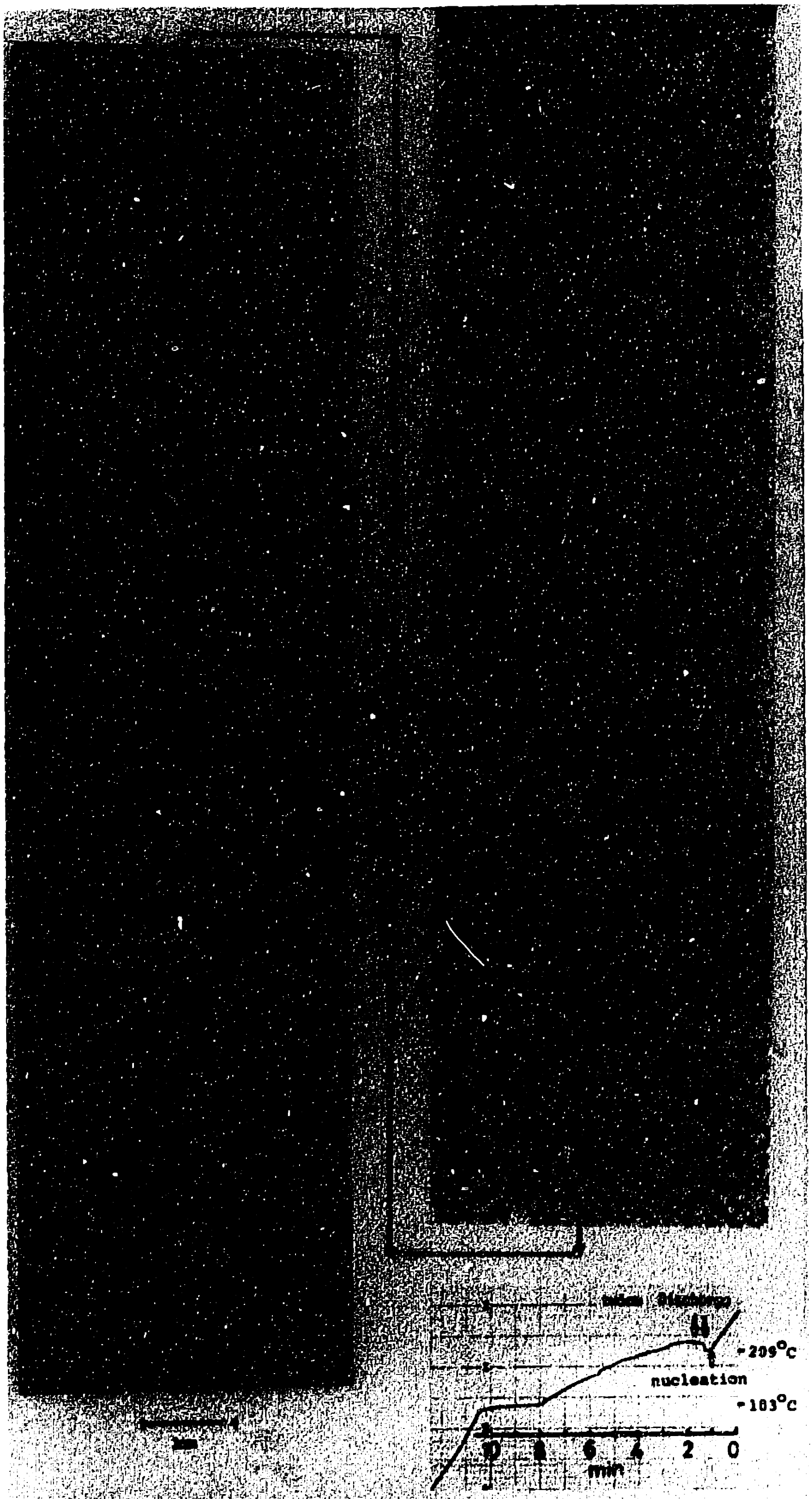

Fig. 8 The solidification structures and the cooling curve which were obtained by discharge at 3200V at 10 and 30 sec after nucleation point.

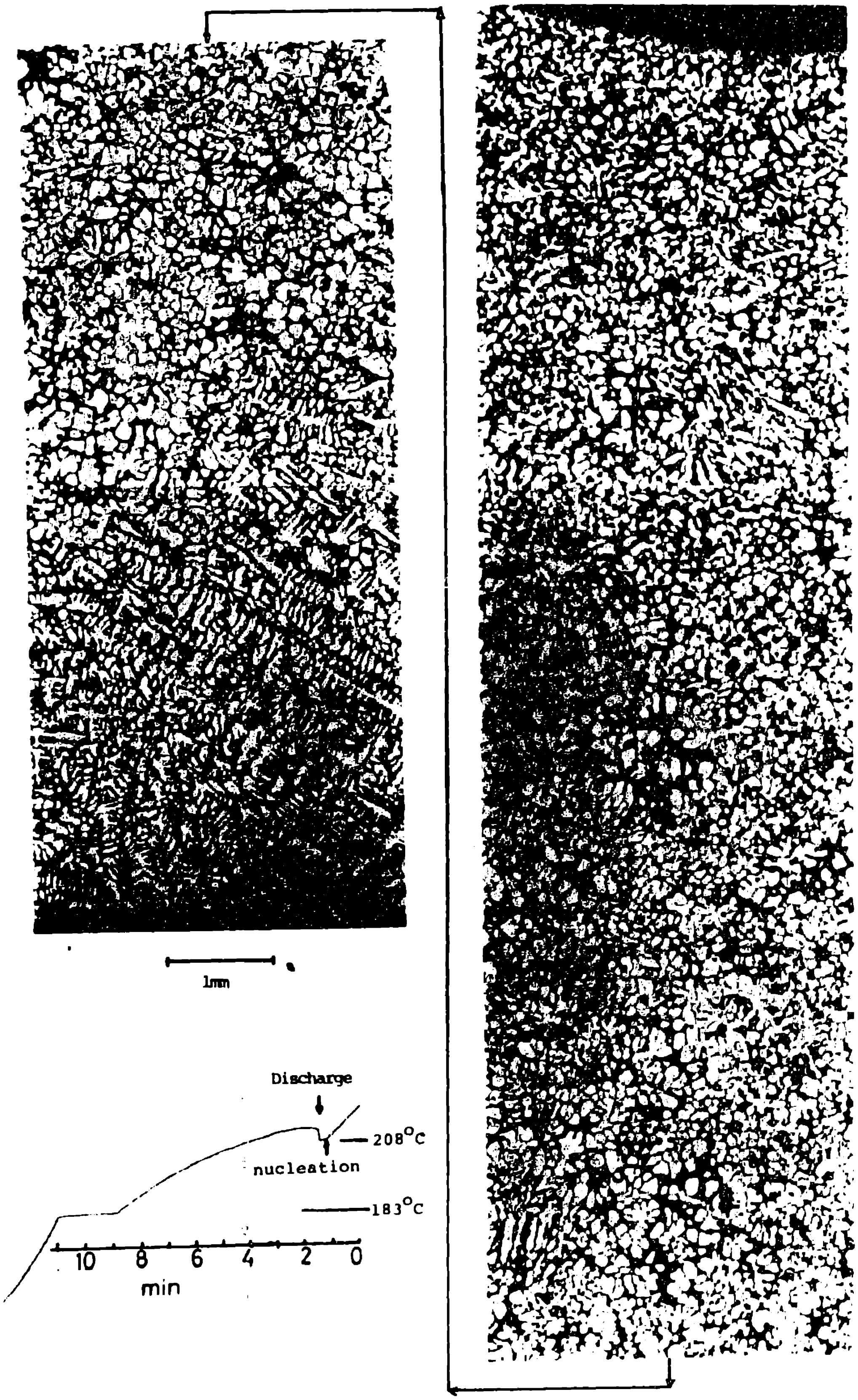

Fig.9 The solidification structures and the cooling curve which were obtained by discharge at 3200V at 15sec after nucleation.

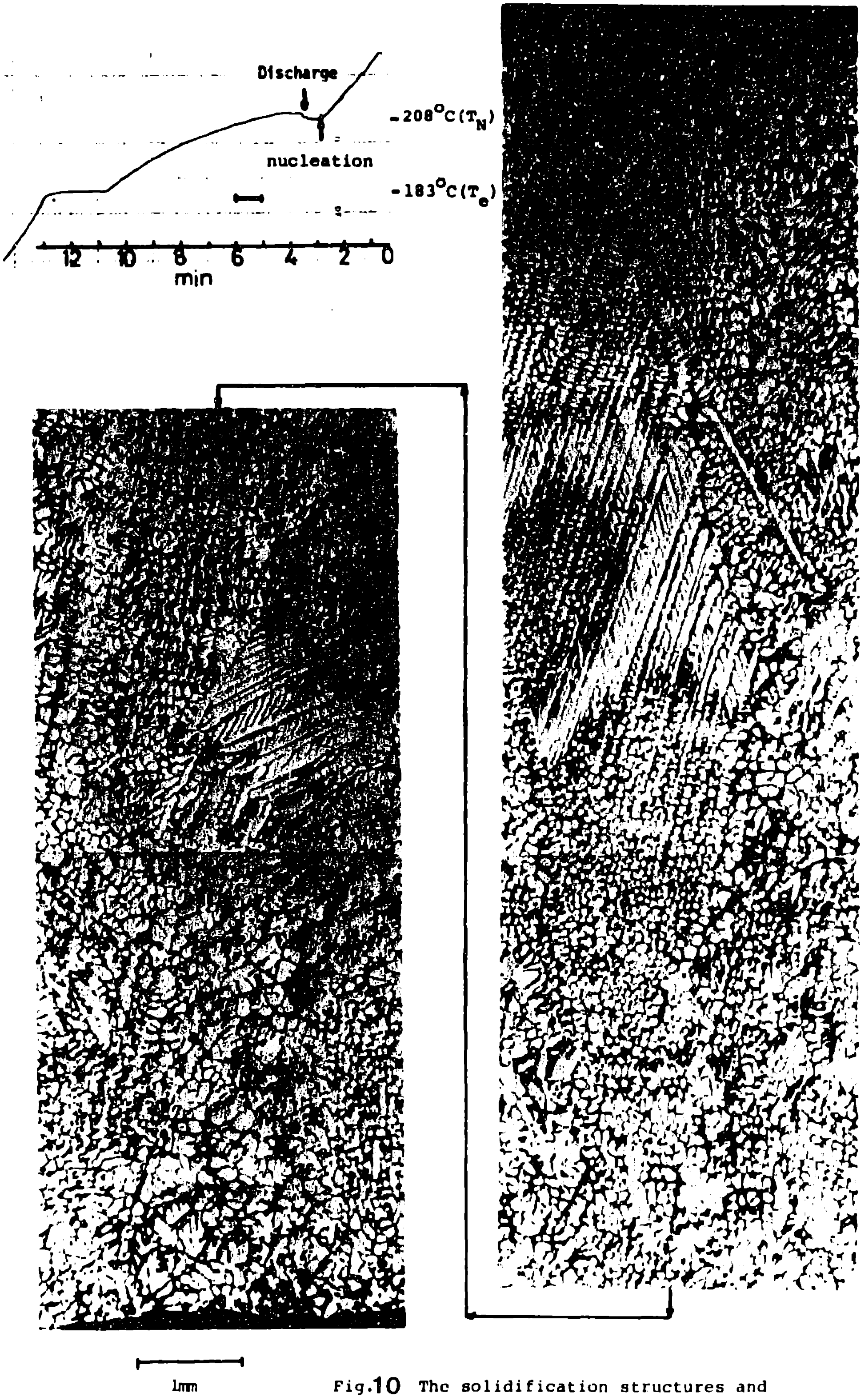

Fig.10 The solidification structures and the cooling curve which were obtained by discharge at 3200V at 30sec after nucleation.

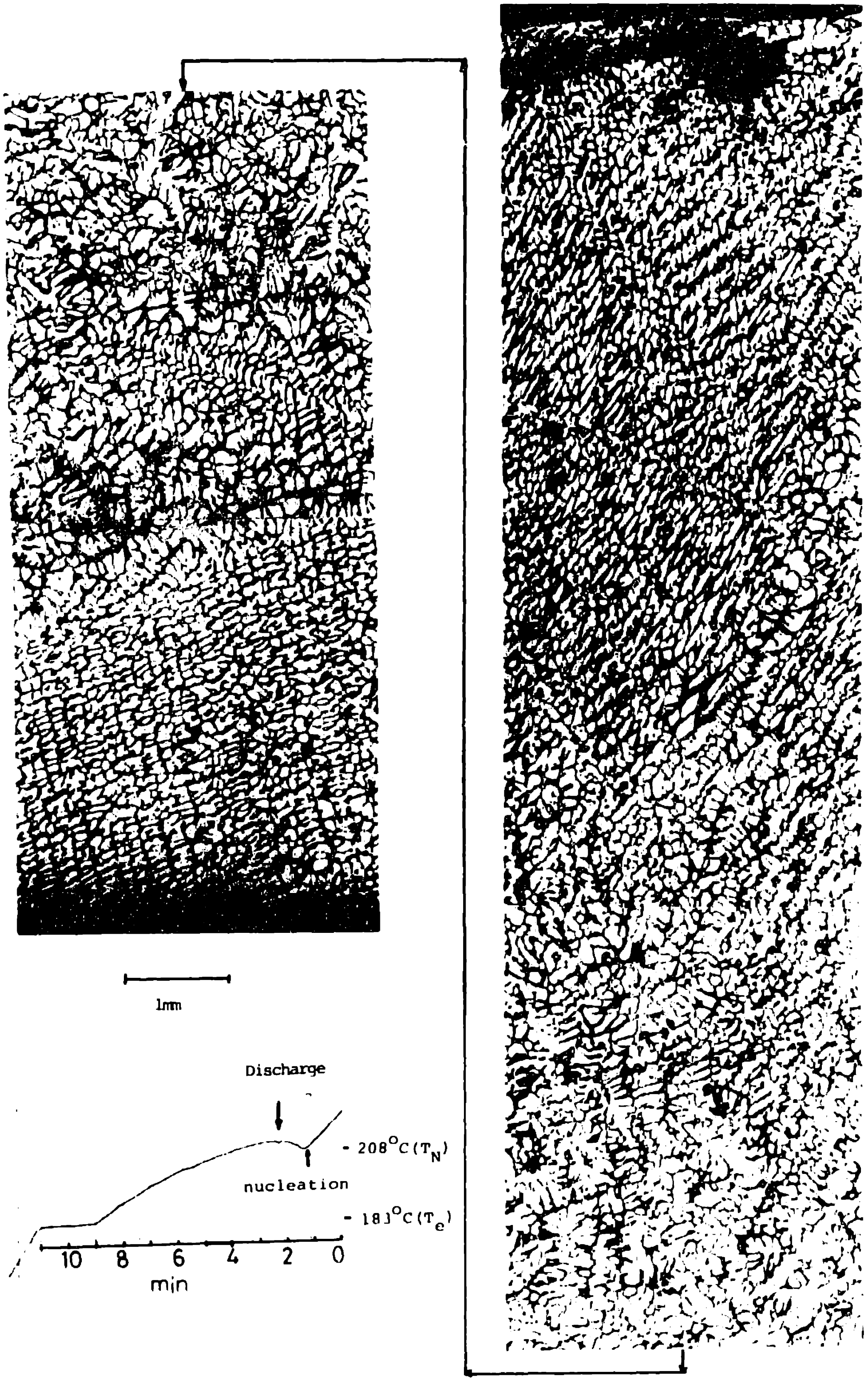

Fig.11 The solidification structures and cooling curve which were obtained by discharge at 3200V at 50sec after nucleation.

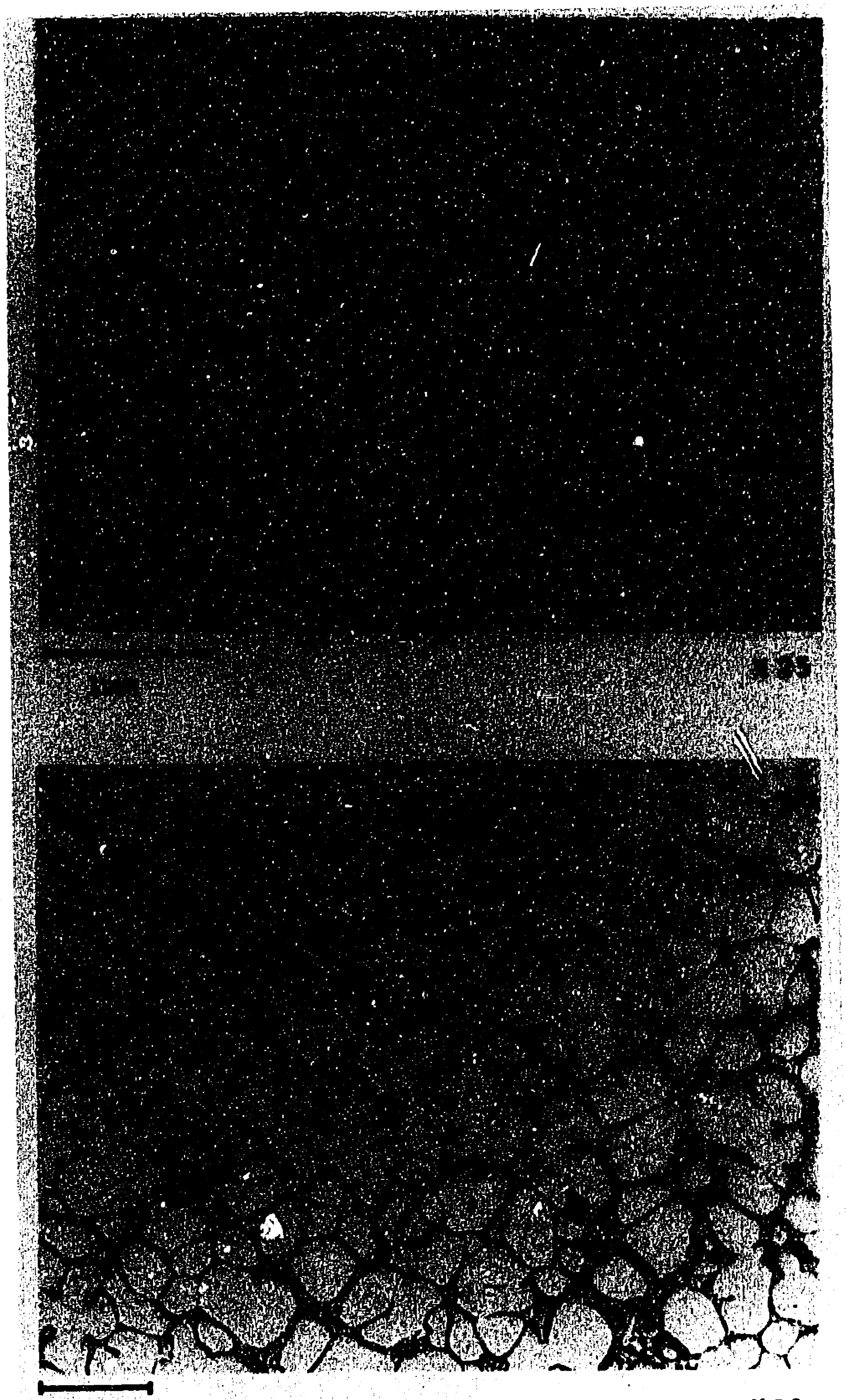

Fig.12 Examples of globular structures of primary phase which was modified due to discharge.

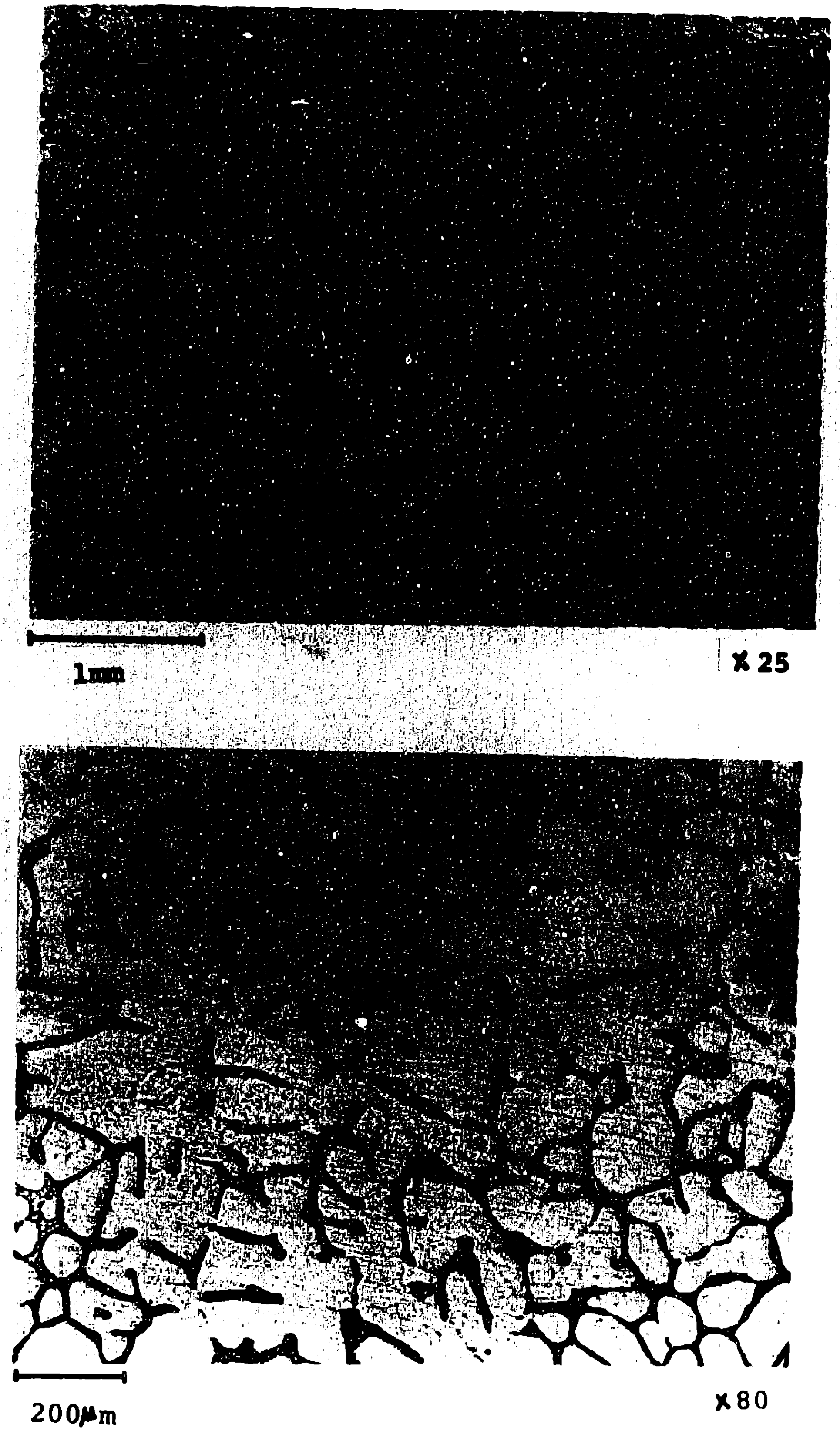

Fig.13 Examples of transient structures of primary phase which was not modified enough by discharge.

Fig.14 Examples of dendritic structures of primary phase which was not modified at all.

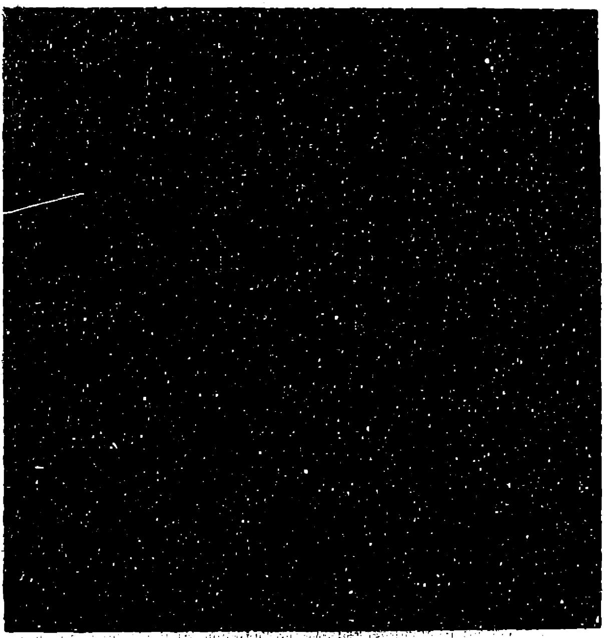

Naturally solidified specimen

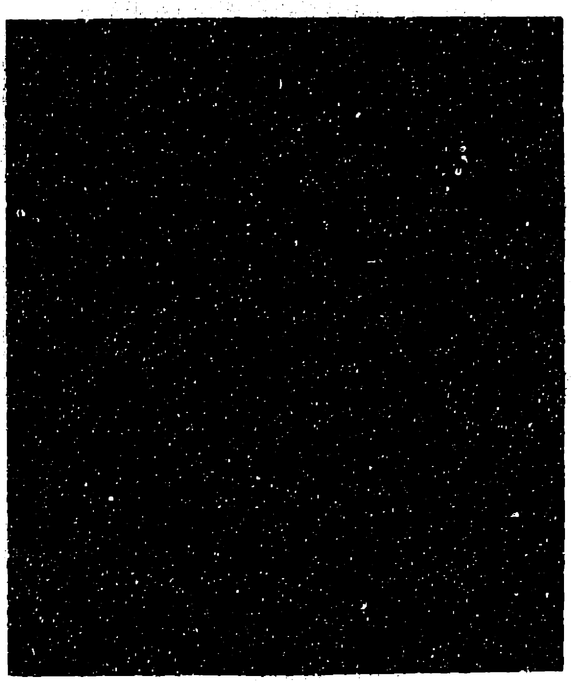

Discharged at 3200V at 15sec
after nucleation (Once)

Fig.15 The comparison of macroscopic structures between naturally solidified and discharged specimens

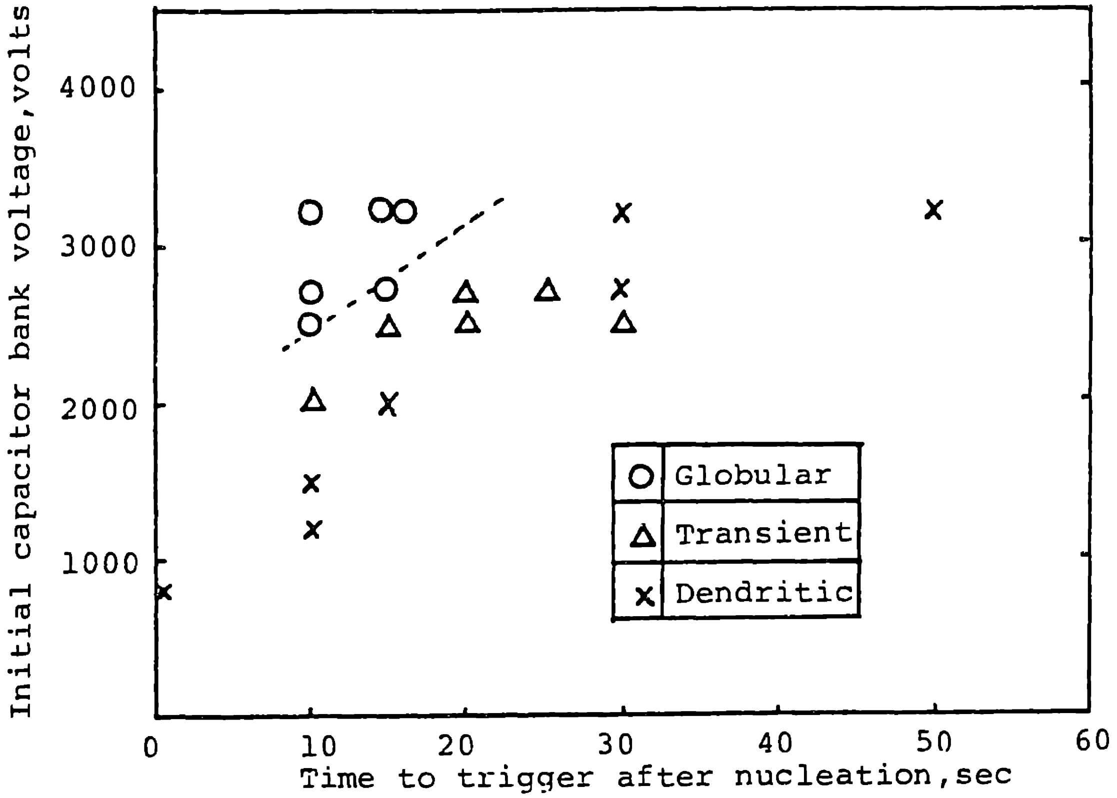

Figure 16 The effect of initial capacitor bank voltage and time to trigger after nucleation on solidification structures.
(Cooling rate befor nucleation was 10.3~11.7°C/min)

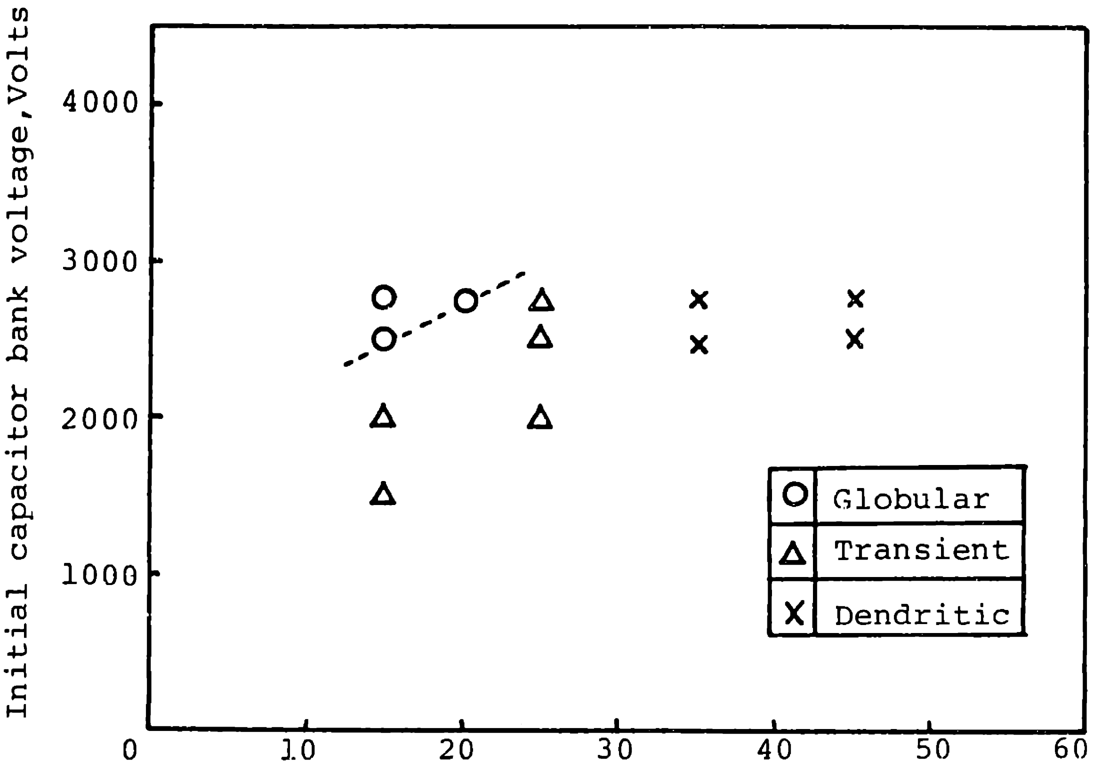

Figure 17 The effect of initial capacitor bank voltage and time to trigger after nucleation on solidification structures.
(Cooling rate before nucleation was 5.8~6.3°C/min)

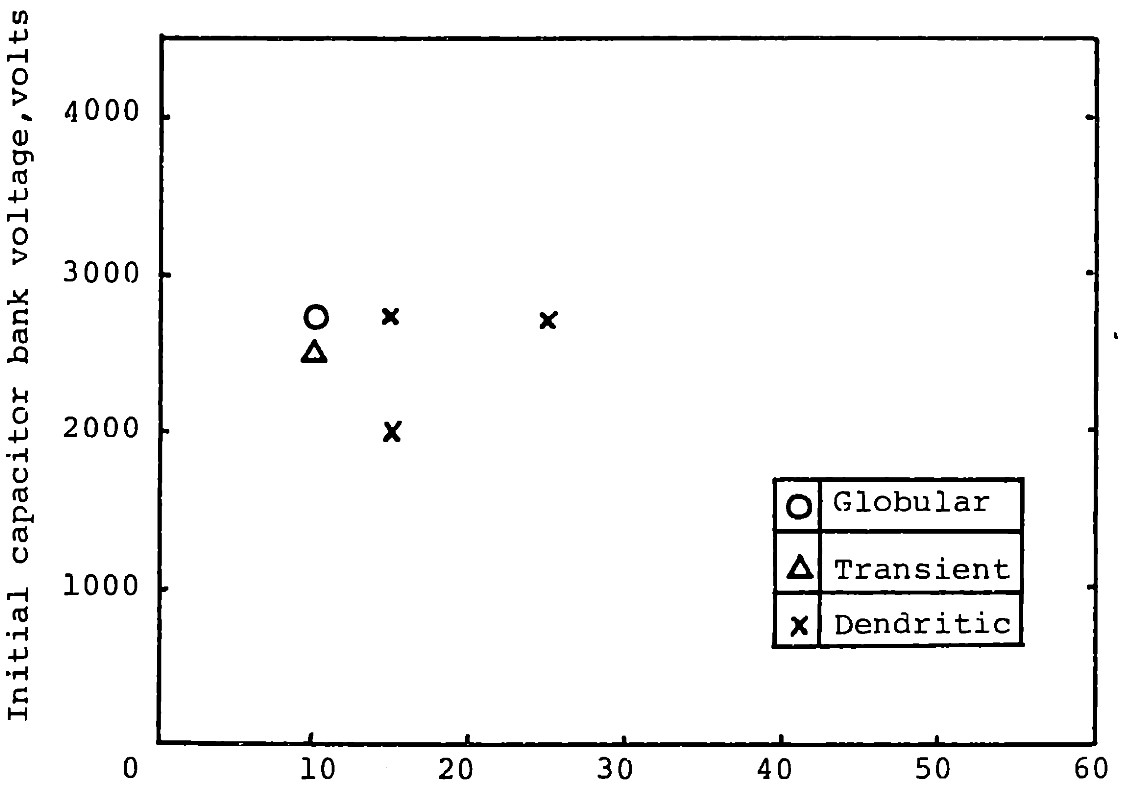

Figure 18 The effect of initial capacitor bank voltage and time to trigger after nucleation on solidification structures.
(Cooling rate before nucleation was 17~19°C/min)

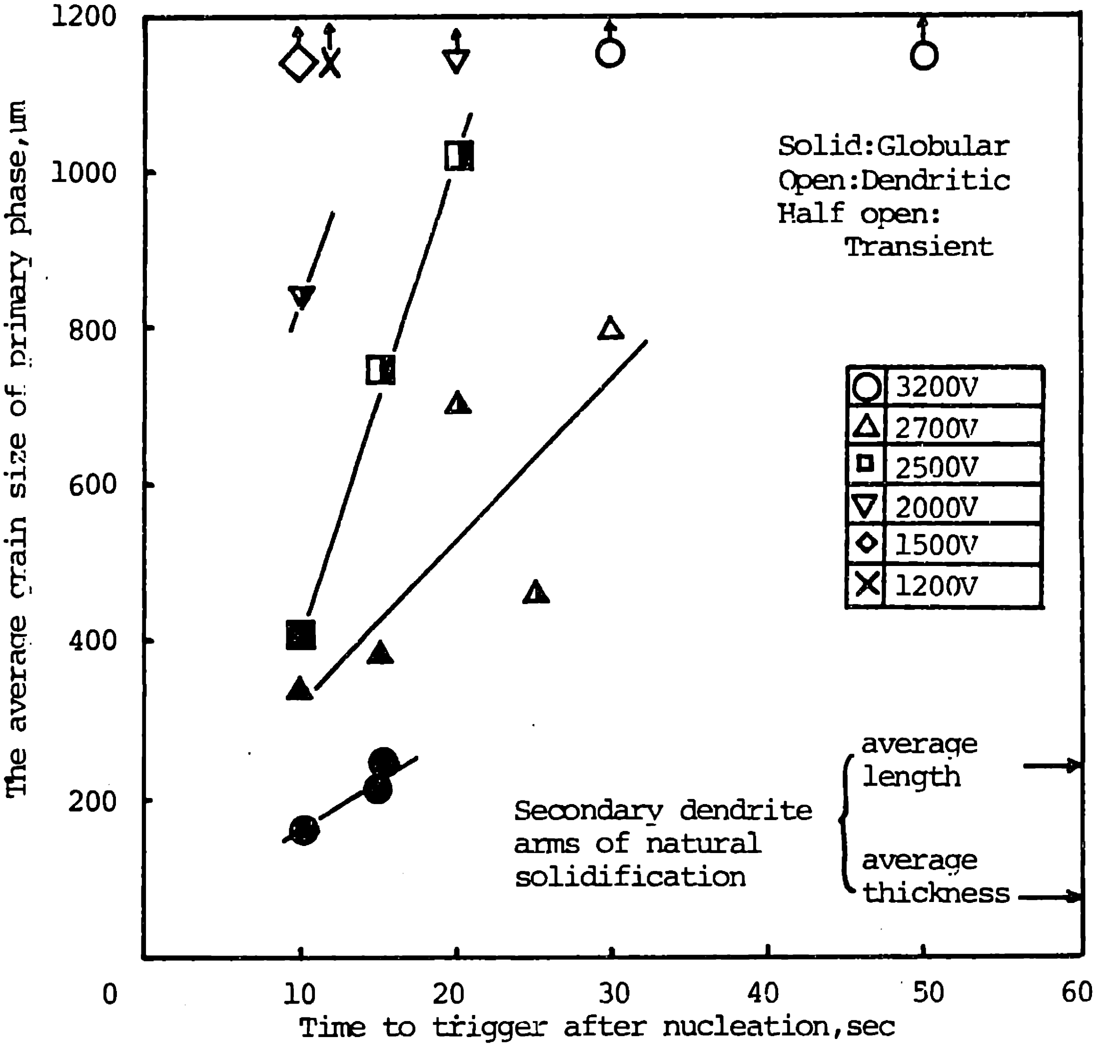

Fig. The relationship among the average grain size of primary phase, time to trigger after nucleation and initial capacitor bank voltage.

(Cooling rate before nucleation = 10.3~11.7°C/min)

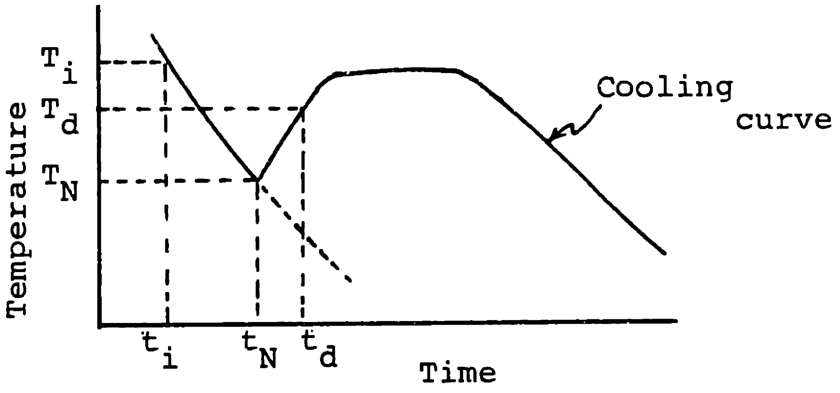

Figure 20 Schematic illustrating of the cooling curve to define parameters for the calculation of fraction of solid.

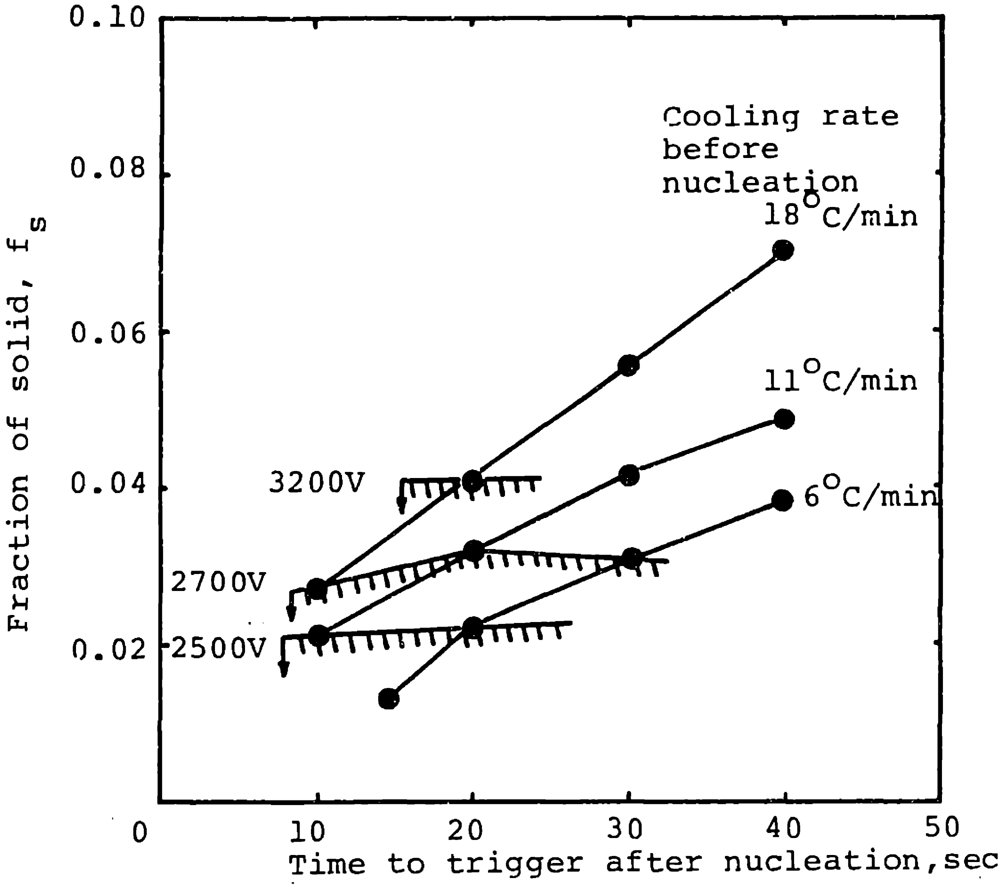

Figure 21 Fraction of solid vs. time to trigger after nucleation. The limit to obtain globular structures due to discharge for different initial voltages are shown in the shadow area.

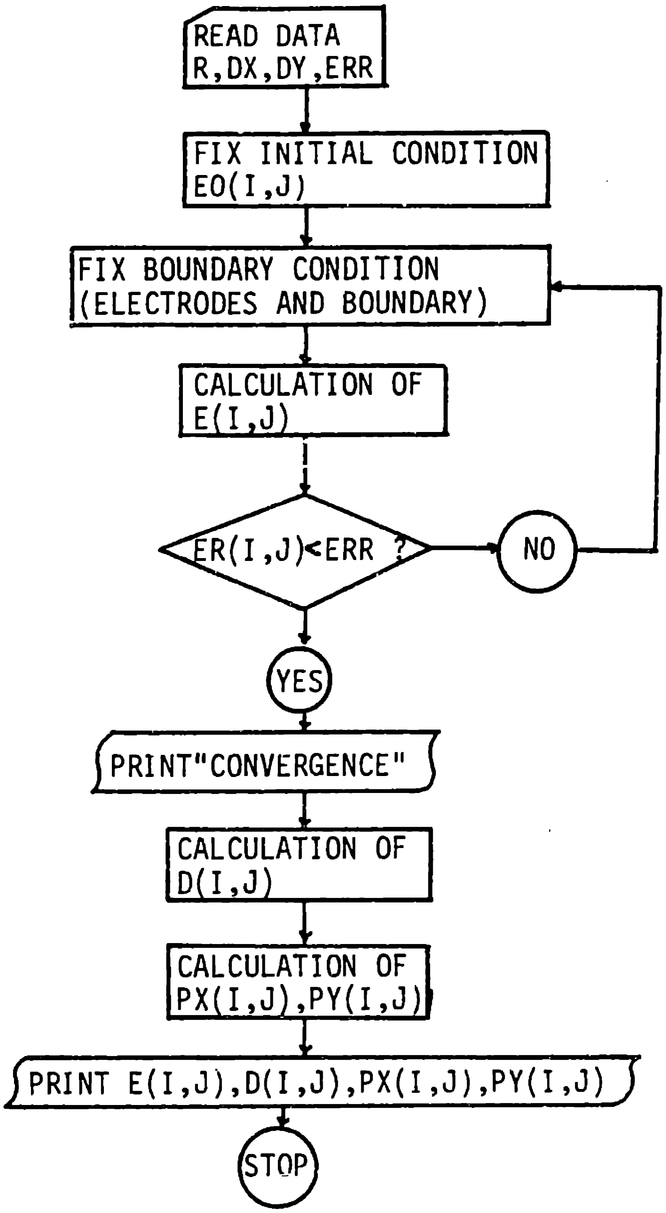

Figure 22 Flow chart for computer calculation for pinch force.

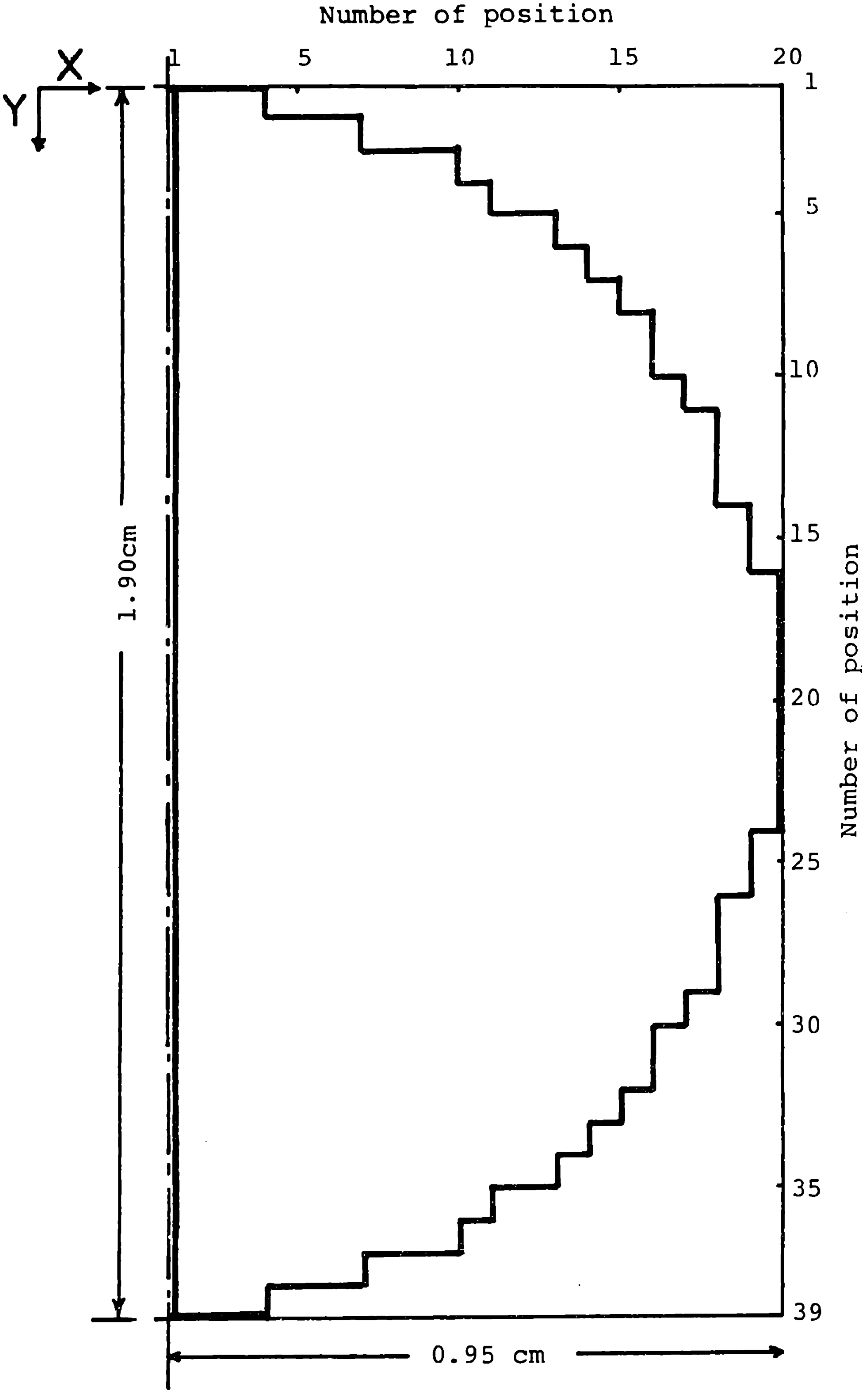

Figure 23 The area for numerical calculation (simulation for a half circle)

1)Measured voltage drop across the sample

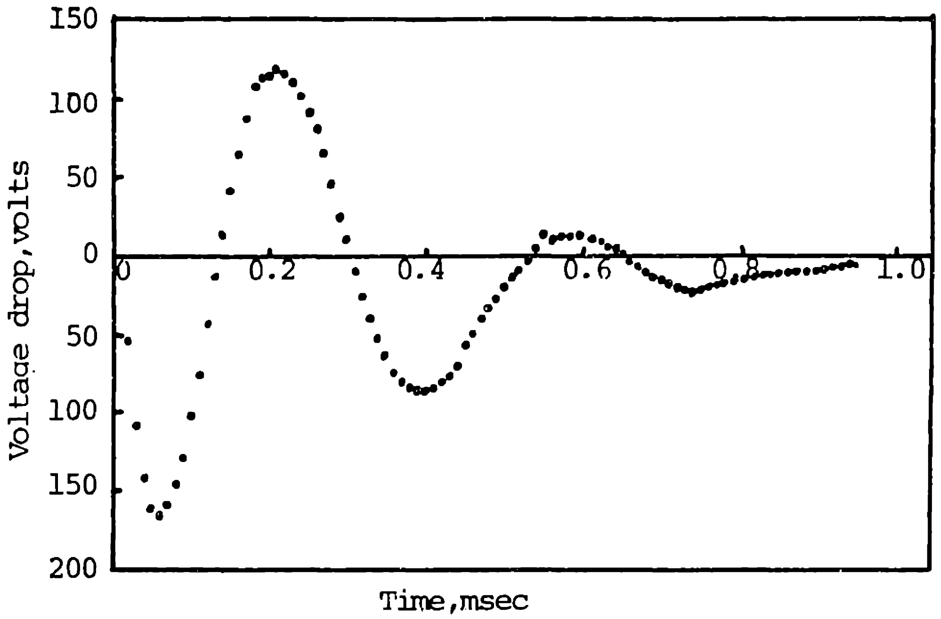

2)Actual voltage drop due to resistance after taking the effect of inductance into account

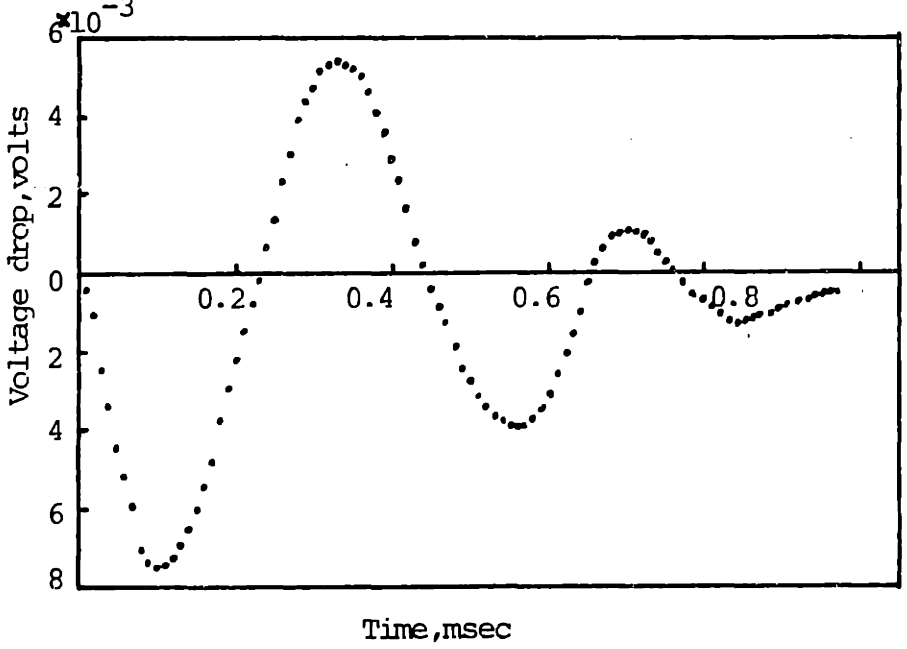

Figure 24 Measured voltage drop across the sample and the actual voltage drop due to resistance after taking the effect of inductance into account.
(Discharged at 2500V at 210°C)

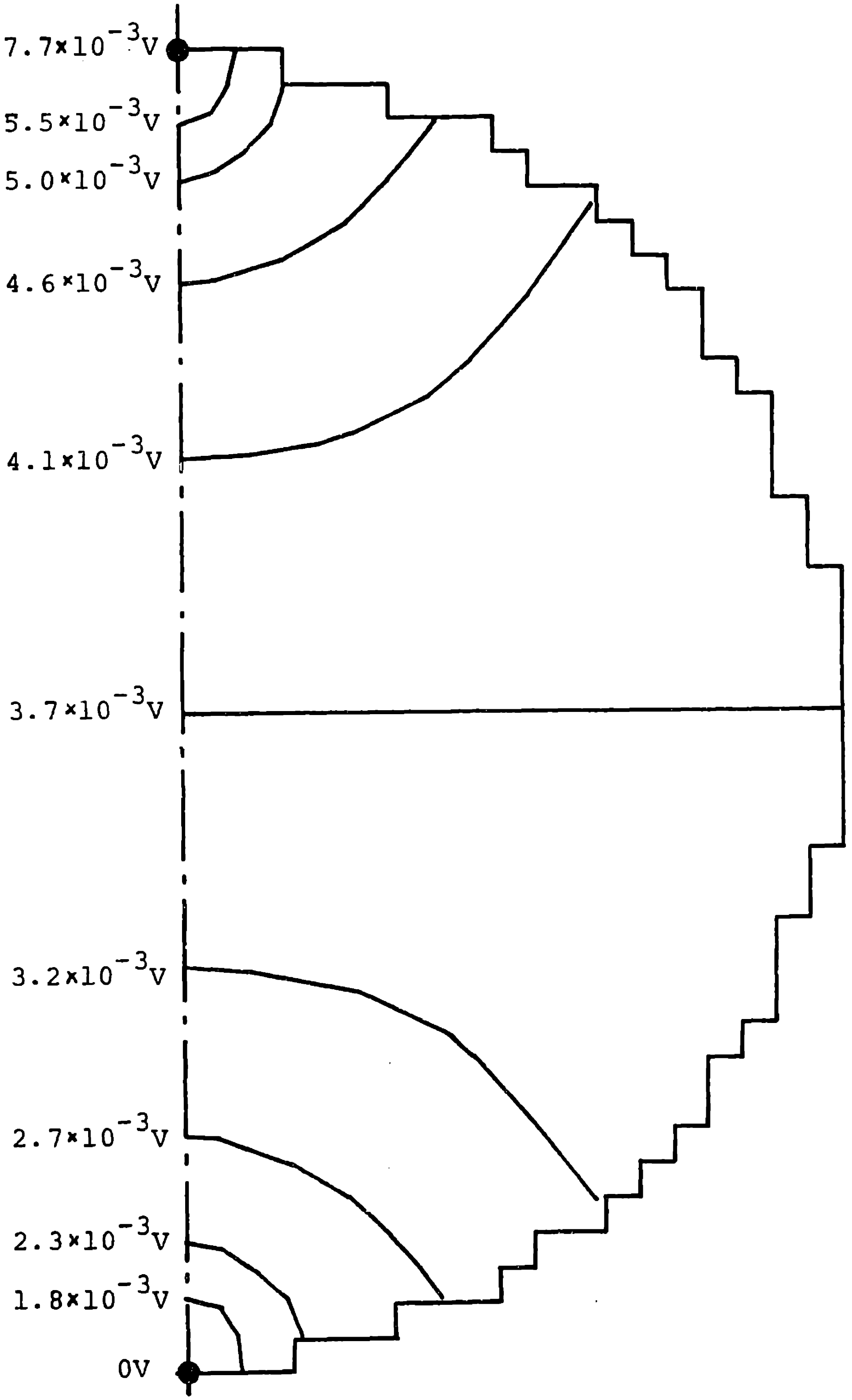

Figure 25 Calculated voltage drcp distribution (Discharged at 2500V at 210°C)

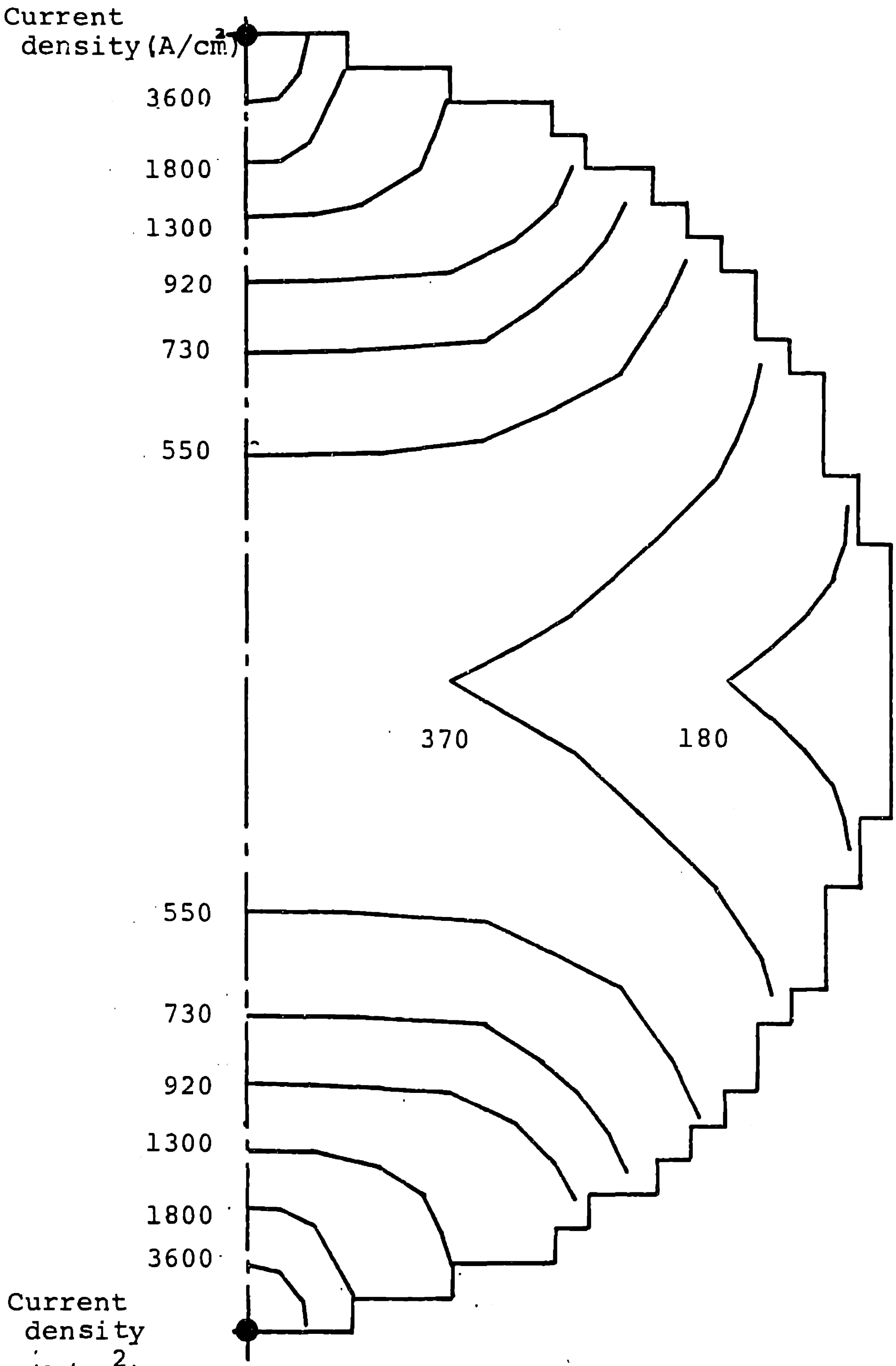

Figure 26 The calculated current density distribution. (Discharged at 2500V at 210°C)

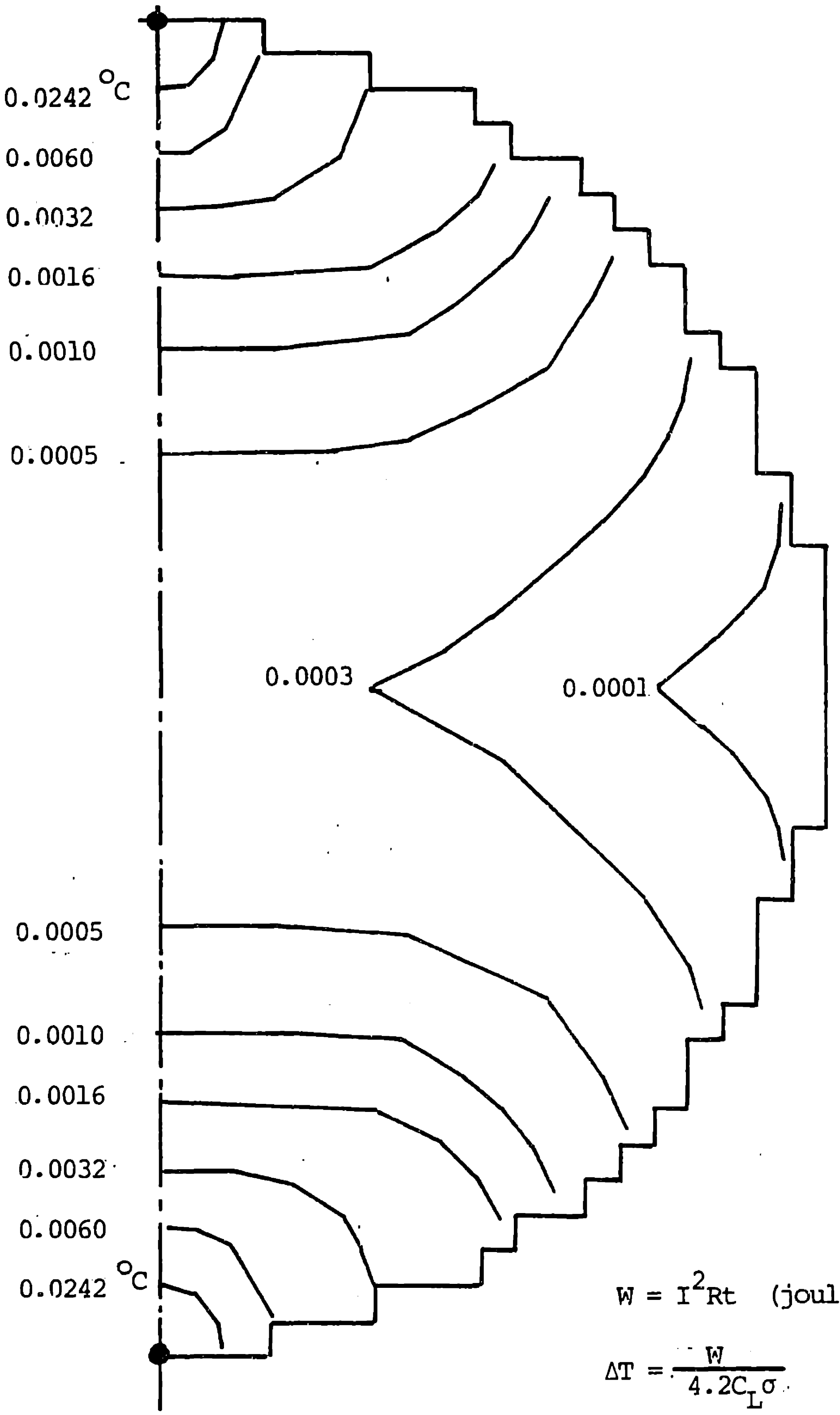

$W = I^2Rt$ (joule)

$$\Delta T = \frac{W}{4.2C_L\sigma}$$

Figure 27 Estimated temperature increase after discharge assuming heat flow is zero. (Discharged at 2500V at 210°C)

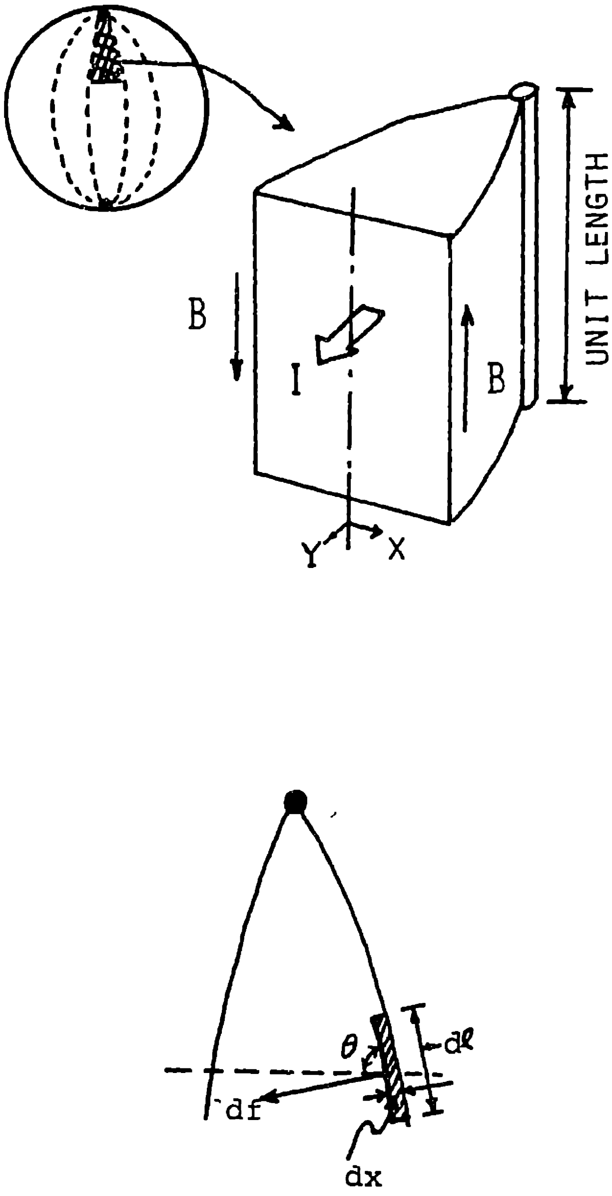

Fig.28 Two kinds of volume elements used for calculations of pinch force.

Top figure is for calculation of magnetic density at a certain point.
Bottom figure is for calculation of interaction between magnetic field and current

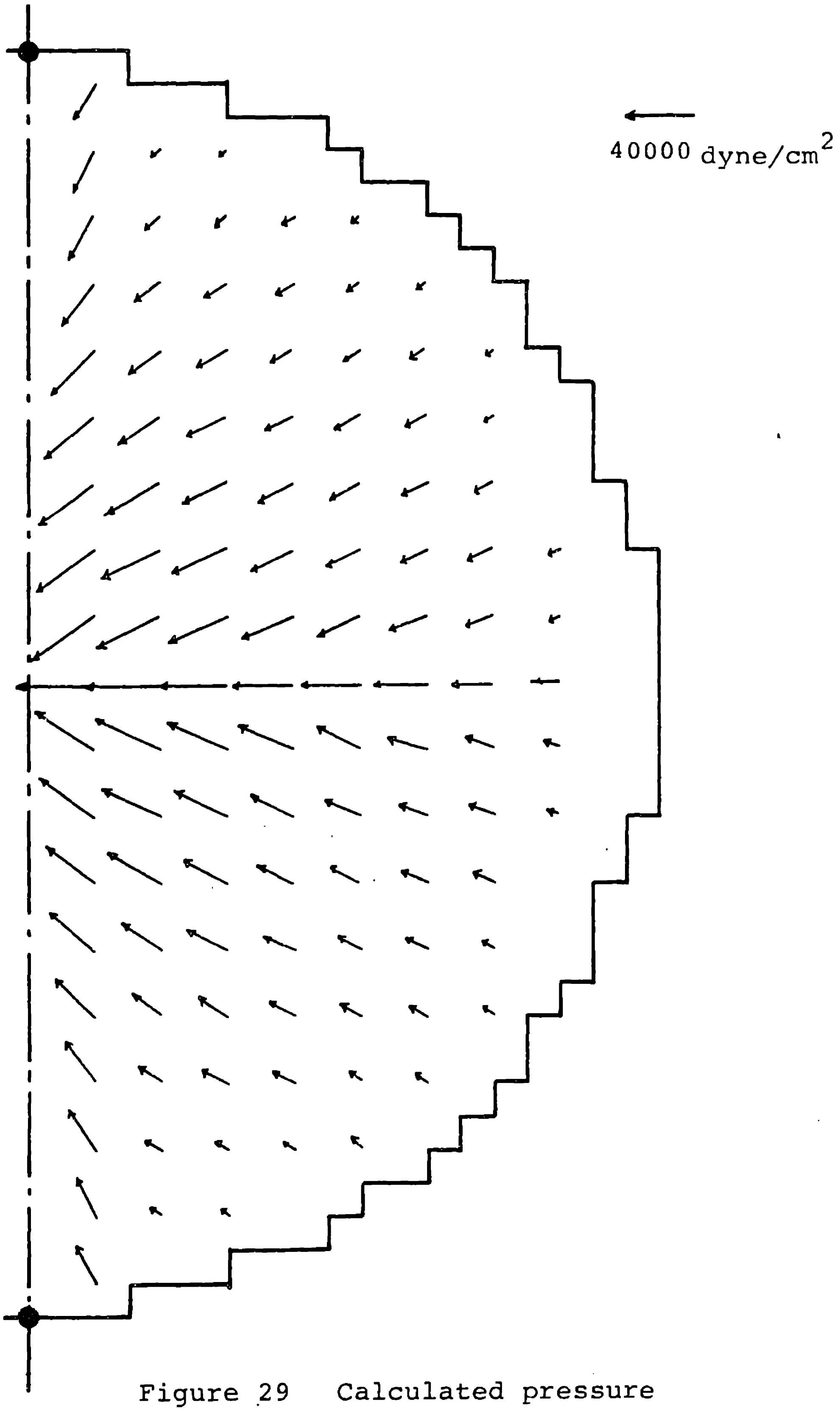

Figure 29 Calculated pressure distribution due to pinch force.

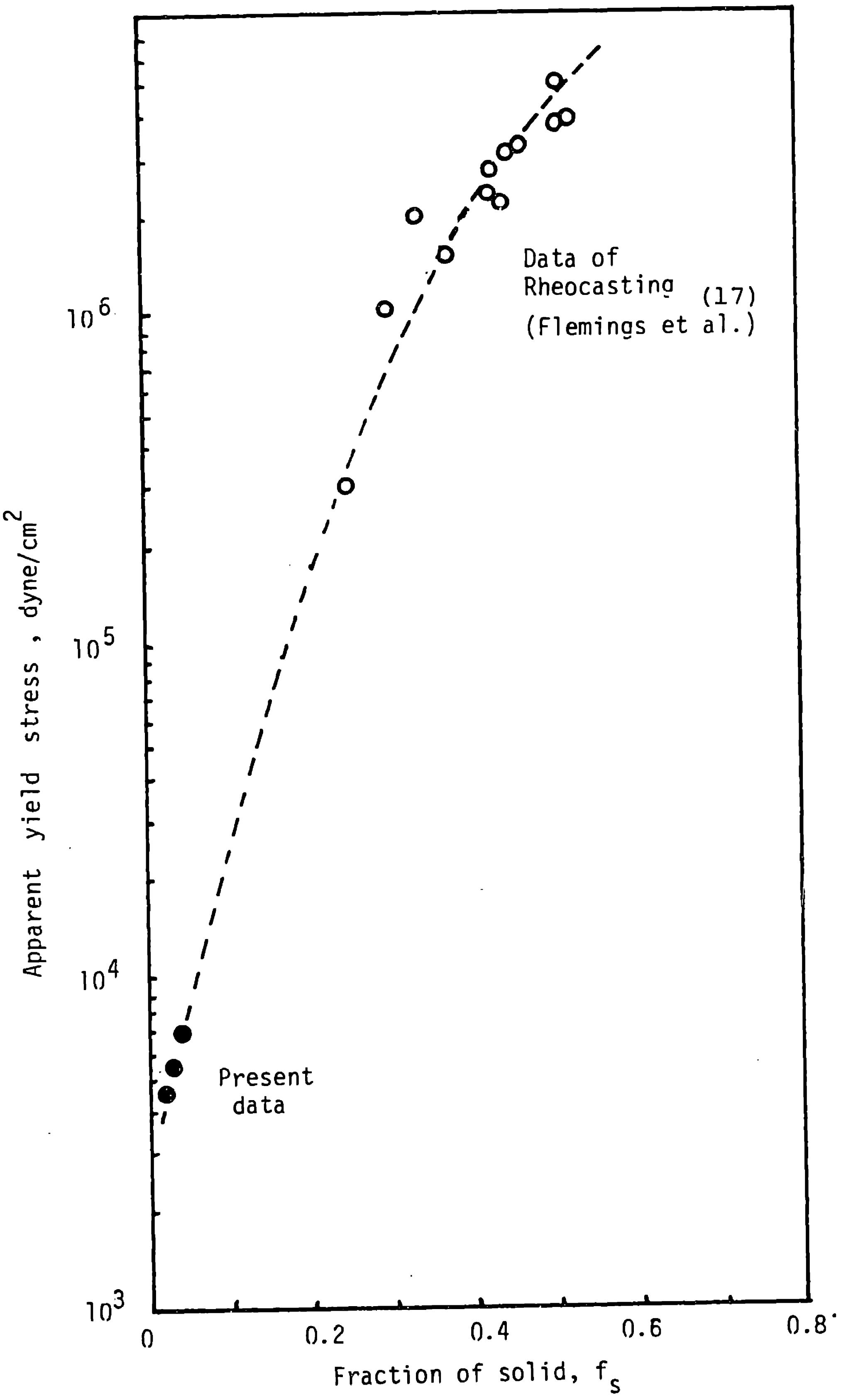

Figure 30 Apparent yield stress vs. fraction of solid. The data from the Rheocasting process are shown for comparison.

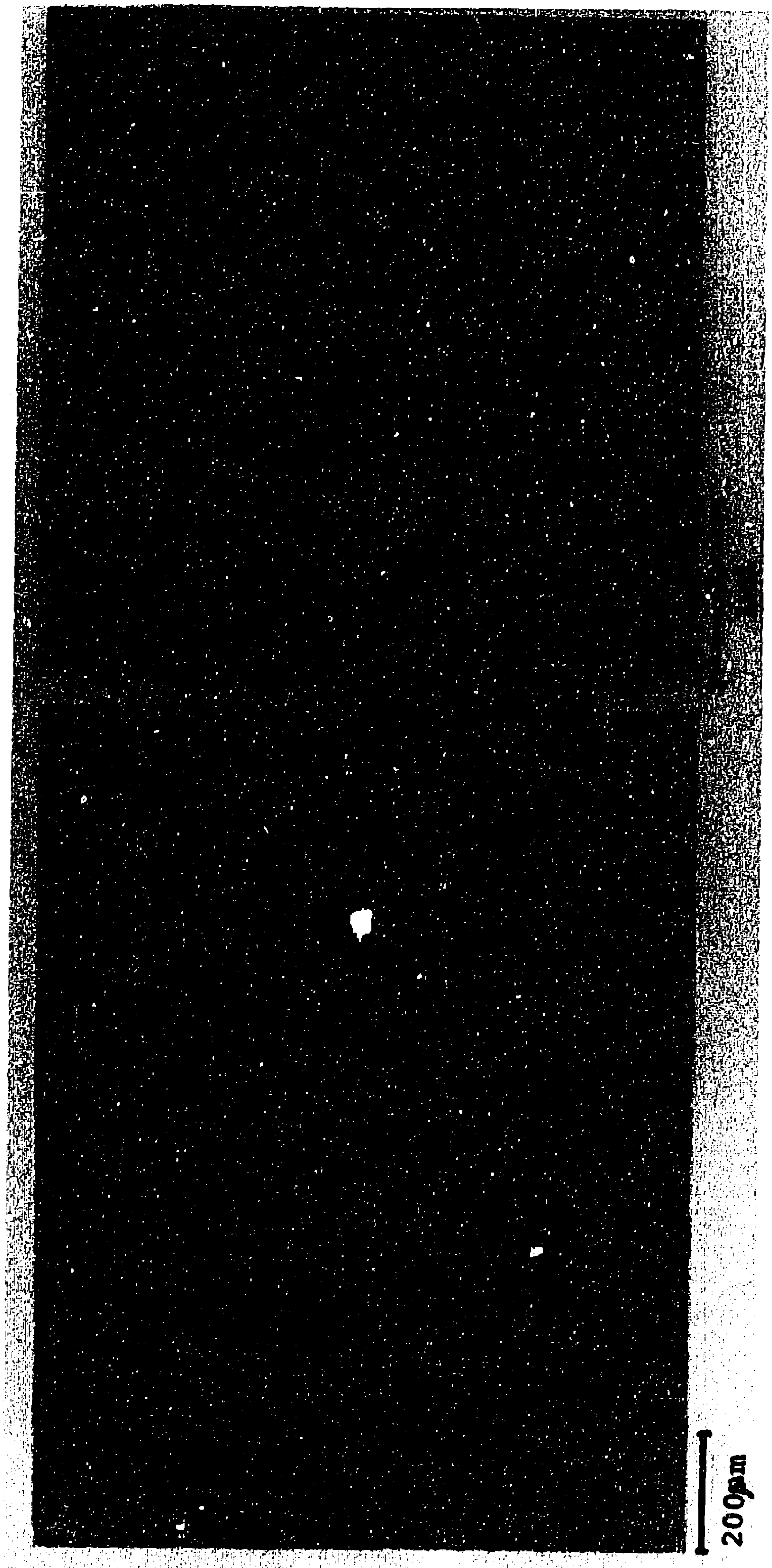

Fig.31 Transient structures.

Appendix 1

How to calculate Θ at a certain point in the specimen is described here.

Assume the potential lines are parts of circles

$$(X+C)^2 + Y^2 = A^2$$

$$\mathrm{Tan}\Theta = \frac{\partial Y}{\partial X}$$

$$\mathrm{Tan}\Theta = -\frac{X+C}{Y} = -\frac{\sqrt{A^2-Y^2}}{Y}$$

$$\Theta = \mathrm{ARCtan}\left(-\frac{\sqrt{A^2-Y^2}}{Y}\right)$$

where X,Y are kown and C,A can be calculated with the positon of electrodes and (X,Y)

Θ:Angle of potential line at a point
A:Radii of a circle
C:Position of center of a circle in X axis
X,Y:Position in the specimen

Appendix 2

Estimation of total resistance of a spcimen

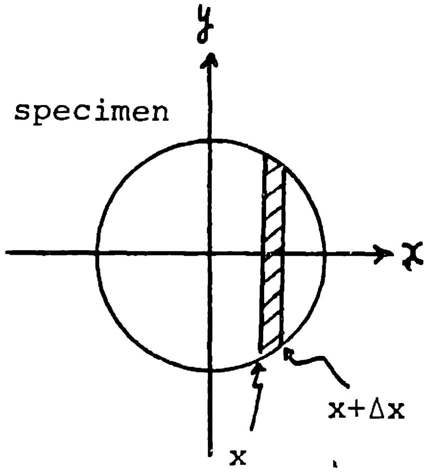

$$R = \rho \frac{\ell}{s} \qquad \ell = \Delta x$$

$$s = 2\sqrt{a^2 - x^2}$$

$$\Delta R = \frac{\rho}{2} \frac{\Delta x}{\sqrt{a^2 - x^2}}$$

$$dR = \frac{\rho}{2} \frac{dx}{\sqrt{a^2 - x^2}} \qquad \int_0^R dR = \frac{\rho}{2} \int_{-a}^{a} \frac{dx}{\sqrt{a^2 - x^2}}$$

$$R = \frac{\rho}{2} \left[\frac{1}{\sin\frac{x}{a}} \right]_{-a}^{a} = 1.19\rho$$

Where

R:total resistance of specimen per unit height
ρ:resistivity of specimen
ℓ:length
s:area
a:radius of the spcimen
x:distance

Appendix 3

Table.1 The coditions of discharging,average grain size of primary phase,and solidification structures (type 2 cooling)

Voltage	t_d	weight	cooling rate	grain size	structures
3200V	10s	54g	11.7°C/min	173μm	globular
3200	15	60	10.4	205	globular
3200	15	60	11.0	230	globular
3200	30	57	11.3	4500	dendritic
3200	50	60	10.3	3000	dendritic
2700	10	55	11.5	349	globular
2700	15	54	11.7	382	globular
2700	20	59	10.6	702	transient
2700	25	58	10.6	464	transient
2700	30	60	11.0	800	dendritic
2500	10	65	10.6	410	globular
2500	15	64	10.5	755	transient
2500	20	60	11.0	1022	transient
2500	30	65	10.3		dendritic
2000	10	64	10.7	842	transient
2000	15	64	10.8	1400	dendritic
1500	10	54	11.6	2000	dendritic
1200	10	57	11.3	3600	dendritic
800	0	60	11.7		dendritic

Voltage:The initial capacitor bank voltage
td:The time to trigger after nucleation of the primary phase
weight:The weight of specimen
Cooling rate:The cooling rate before nucleation
Grain size:The average grain size of the primary phase
Structure:The solidification structures

Table.2 The conditions of discharging and solidification structures.(type 3 cooling)

Voltage	td	weight	cooling rate	structures
2700V	15s	53g	6.1°c/min	globular
2700	20	60	5.9	globular
2700	25	60	6.1	transient
2700	35	60	6.0	dendritic
2700	45	60	5.9	dendritic
2500	15	59	6.0	globular
2500	25	57	6.1	transient
2500	35	64	6.0	dendritic
2500	45	65	6.0	dendritic
2000	15	60	5.8	transient
2000	25	66	6.3	transient
1500	15	71	6.3	transient

Table.3 The conditions of discharging and solidification structures.(type 1 cooling)

voltage	td	weight	cooling rate	structures
2700V	10s	64g	17°c/min	globular
2700	15	66	18	dendritic
2700	25	61	19	dendritic
2500	10	63	19	transient
2000	15	67	19	dendritic

References

1) O.Haida, H.Kitaoka, Y.Habu, S.Kakihara, H.Bada, and S.Shiraishi; Trans. ISIJ, vol.24, 1984, P891

2) H.Mizukami, M.Komatsu, T.Kitagawa, K.Kawakami; Trans.ISIJ, vol.24, 1984, P923

3) K.A.Jackson: Trans. AIME, 236 (1966), P149

4) S.O'hara and W.A.Tiller; Trans. AIME., 239 (1967), P497

5) W.C.Johnston, G.R.Katler, S.O'hara, H.V.Ashcomb and W.A.Tiller; Trans. AIME, 233 (1965), P1856

6) W.A.Tiller, S.O'hara; "Solidification of Metals", Iron and Steel Inst. Pub.No.110, 1968, P27

7) A.Vogel; Met. Sci, 12 (1978), P576

8) R.D.Doherty; Mater. Sci. and eng., 65 (1984), P181

9) R.P.Doherty; Met. Sci, 16 (1982), P1

10) A.Vogel and B.Cantor; J. of Cryst. Growth, 37 (1977), P309

11) A.Cibula; J. Inst. Metals, 76 (1949), P34

12) R.T.Southin; J. of the Australian Inst. of Metals, 10 (1965), P115

13) J.G.Kura and H.W.Mishler; Battle Memorial Inst. Memorandum, No.166, May15, 1963

14) K.F.Alder; The Australian Eng., Dec8, 1952, P53

15) E.A.Hiedemann; J. of Acoust. Soc. Amer, 26 (1954), P831

16) Tesman; MetalProgress, 79 (1961), P79

17) D.B.Spencer, R.Mehrabian, and M.C.Flemings; Met. Trans. 3 (1972) P1925

18) R.Mehrabian and M.C.Flemings: Trans. Am. Foundrymen's Soc. 80 (19722), P173

19) E.F.Fascetta, R.G.Rick, R.Mehrabian and M.C.Flemings; Trans. Am. Foundrymen's Soc. 81 (1973), P95

20) K.P.Young, R.G.Rick, J.F.Boylan, R.L.Bye, B.E.Bond and M.C.Flemings; Trans. Am. Foundrymen's Soc., 84 (1976), P169

21) T.Matsumiya, M.C.Flemings; Met. Trans B, 123 (1981), P17

22) V.Laxmann, M.C.Flemings; Met. Trans. A, 11A (1980), P1927

23) P.A.Joly and R.Mehrabian;J.of Met. Sci., 11 (1967), P1373

24) T.Z.Kattamis, J.C.Coughlin and M.C.Flemings; Trans. AIME, 239 (1967), P1504

25) M.Kahlweit; Scripta Met. 2 (1968), P251

26) M.C.Flemings; Solidification Processing, MacGrow Hill

27) T.Z.Kattamis, and M.C.Flemings; Trans. AIME, 236 (1966), P1523

28) T.Z.Kattamis, and M.C.Flemings; Mod. Cast, 52 (1967), P97

29) T.Z.Kattamis, and M.C.Flemings; Trans. Am. Foundrymen's Soc. 75 (1967), P191

30) T.Z.Kattamis, and Flemings; Metall. Trans, 1 (1970), P1449

31) P.Haasen; Physical Metallurgy, Cambridge Univ.Press, P56

32) D.A.Porter, and K.E.Eastering; Phase Transformation in Metals and Alloys, Van Nostrand Reinhold, P186

33) A.Hellawell; Solidification and Casting of Metals, P161

34) J.V.Wood; ibid, P179

35) Robert.M.Frano, and Lan J.Chu, Richard.B.Adler; "Electromagnetic Field, Energy, and Forces", John Wiley and Son, Inc.

36) Dale.R.Crson, Paul Lorrain; "Introdution to electromagnetic field and waves"

37) Parry Moon, and Domina E. Spencer; "Foundation of Electrodynamics"